

E.T.S. de Ingeniería Industrial,
Informática y de Telecomunicación

Electrospinning of superhydrophobic
nanocomposite films for corrosion protection
of aluminum substrates



Grado en Ingeniería
en Tecnologías Industriales

Trabajo Fin de Grado

Autor: Álvaro Iribarren Zabalegui

Directores: Dr. Pedro José Rivero Fuente y Dr. Carlos
Berlanga Labari.

Pamplona, Enero 2019

ABSTRACT

In this work, the electrospinning technique is used for the synthesis of micro/nanofibers using a polymeric precursor with hydrophobic (even superhydrophobic) behaviour such as polystyrene (PS) or polyvinyl chloride (PVC). These electrospun fibers are deposited onto aluminum substrates (6061T6). The effect of varying the different electrospinning deposition parameters (mostly applied voltage and flow-rate) will be exhaustively analyzed in order to optimize the resultant electrospun coatings. Several fiber characterization tests have been performed, including Field Emission Scanning Electron Microscopy (FE-SEM), Atomic Force Microscopy (AFM), Thermogravimetric analysis (TGA), Differential Scanning Calorimetry (DSC), Optical Microscopy (OM) and Water Contact Angle (WCA) measurements. Furthermore, the anti-corrosion properties of these electrospun coatings can be enhanced by the addition of metal oxide nanoparticles (ZnO) that act as corrosion inhibitors. Finally, electrochemical corrosion tests (Tafel and pitting tests) have been performed, showing an improvement in the resultant corrosion resistance of the aluminum alloys coated by the combination of both polymeric films with metal oxide inorganic nanoparticles.

Keywords

- Electrospinning
- Superhydrophobic
- Corrosion
- Micro/nanofibers
- Polyvinyl chloride (PVC)
- Polystyrene (PS)
- Metal oxide nanoparticles

INDEX OF CONTENTS

CHAPTER 1	6
1. INTRODUCTION	7
CHAPTER 2	8
2. STATE OF THE ART.....	9
2.1. Electrochemical corrosion.....	9
2.2. Corrosion costs	10
2.3. Corrosion on aluminum, pitting corrosion	13
2.4. Anti-corrosion techniques	14
2.5. Hydrophobicity, super-hydrophobic coatings	15
CHAPTER 3	17
3. ELECTROSPINNING TECHNIQUE.....	18
3.1. Fundamentals	18
3.2. Electrospinning parameters	19
3.2.1. Processing parameters.....	19
3.2.1.1. Applied voltage.....	19
3.2.1.2. Flow rate.....	20
3.2.1.3. Distance between capillary and collector	20
3.2.2. Solution parameters	21
3.2.2.1. Polymer concentration.....	21
3.2.2.2. Solvent volatility	21
3.2.2.3. Solution conductivity	21
3.3. Why electrospinning?.....	22
CHAPTER 4	23
4. MATERIAL SELECTION.....	24
4.1. Polymer selection: PS and PVC.....	24
4.2. Required solvents.....	25
4.3. Metal oxide nanoparticles, ZnO.....	26
4.4. List of purchased reagents.....	27
CHAPTER 5	28
5. EXPERIMENTAL PROCEDURE.....	29
5.1. Optimization of the electrospinning parameters	29
5.1.1. Polymer solution preparation.....	29
5.1.2. Fiber deposition at different applied voltages and flow rates	31
5.1.3. Fiber characterization	32
5.1.3.1. Fiber diameter measurements.....	32
5.1.3.2. Water Contact Angle (WCA) measurements	39

5.2. Corrosion inhibitor (ZnO) addition	43
5.2.1. Solution preparation.....	43
5.2.2. Electrospinning of the composite mixtures	44
5.2.3. Characterization of the polymer+ZnO fibers.....	45
5.2.3.1. Thermogravimetric analysis	45
5.2.3.2. Fiber diameter measurements.....	47
5.2.3.3. Water contact angle measurements	49
5.3. Heat treatment	50
5.3.1. Glass transition temperature of PVC and PS	52
5.3.2. Effect of heat treatment on the water contact angle values.....	54
5.3.3. Fiber characterization after heat treatment, AFM and SEM	58
5.3.3.1. Atomic Force Microscopy results	58
5.3.3.2. Scanning Electron Microscopy results	61
5.4. Corrosion tests	63
5.4.1. Tafel polarization test methodology.....	63
5.4.2. Pitting corrosion test methodology	65
5.4.3. Corrosion tests results for bare aluminum.....	65
5.4.4. Corrosion tests results for the PVC nanocomposite coatings	67
5.4.5. Corrosion tests results for the PS nanocomposite coatings.....	71
5.4.6. Overall pitting corrosion tests results	74
CHAPTER 6	76
CONCLUSIONS	77
FUTURE RESEARCH LINES	77
CHAPTER 7	79
5 th Global Nanotechnology Congress and Expo.....	80
1 st Coatings and Interfaces Web Conference.....	82

CHAPTER 1: INTRODUCTION

1. INTRODUCTION

Aluminum (Al) and its alloys (AAs) are widely used in domestic and industrial areas such as automotive, aviation, aerospace and marine industries, due to their physical and mechanical properties: low specific weight, good mechanical properties at low temperatures, good corrosion resistance and excellent thermal and electrical conductivities [1].

The aluminum alloy (AA) used in this work is the 6061T6. It is a precipitation-hardened AA, and further tempered, containing magnesium (Mg) and silicon (Si) as its major alloying elements. This presence of Mg and Si increase the mechanical properties of the alloy. The ideal content of these two elements is around 0.8%.

Some of the common applications of this alloy include bicycle frames, firearm sound suppressors, aircraft components, docks structures... [2].

Although Al and AAs have high corrosion resistance due to the formation of a surface passive layer (Al_xO_y) in air, they can still suffer corrosion when they are exposed to corrosive media for example with aqueous chloride ions [3].

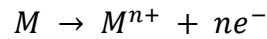
In order to extend the field of applications of these alloys it is necessary to protect them against this electrochemical corrosion.

CHAPTER 2: STATE OF THE ART

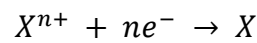
2. STATE OF THE ART

2.1. Electrochemical corrosion

Corrosion can be defined as the deterioration of materials' properties as a consequence of reactions with their environment [4]. The most important of the different corrosion processes is the electrochemical corrosion of metals, in which the oxidation of the metal occurs:



This oxidation is sustained by the consumption of electrons in another reaction:



Since the electrochemical corrosion involves the release of ions to the environment and the movement of electrons within the material, this mechanism can occur only if the environment can contain ions and the material can conduct electrons.

The most important case of electrochemical mechanisms is the corrosion of metals in aqueous solutions. Atoms at the surface of the metal enter the solution as metal ions and electrons move to another site of the metal where they are consumed by species in contact with the metal in order to sustain the reaction (it is a redox process).

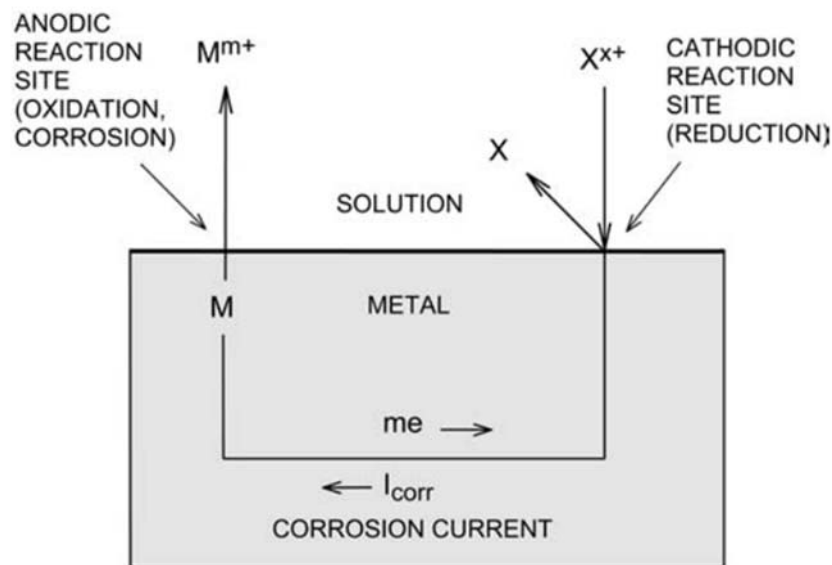


Fig. 1. The basic electrochemical corrosion process [4].

As it can be seen in Fig. 1, the oxidation occurs at the anodic reaction site on the metal surface and this is the location of the loss of metal by corrosion. The electrons move to the cathodic reaction site where they are picked up by substances in contact with the metal surface. The distance between the anodic and cathodic reaction sites may vary greatly, from a few atoms to even meters of distance. When these sites are close and it is difficult to distinguish them uniform corrosion is said to occur, whereas when the sites are well separated and do not change in time localized corrosion is said to occur. In this last case the corrosion can be mainly observed in the anodic area due to the loss of metal.

2.2. Corrosion costs

The economic aspects of corrosion are far greater than most people realize. In 2016, NACE International, a professional technical association dedicated to protecting the environment and reducing the economic impact of corrosion, released the *"International Measures of Prevention, Application and Economics of Corrosion Technology (IMPACT)"* study, in which it estimates the global cost of corrosion to be around 2,5 trillion US\$. This is approximately the 3,4% of the global gross domestic product. According to the study, the implementation of corrosion prevention practices could save around 15-35% of the cost of damage. But the goal is not only to reduce the economic costs, but also to avoid a possible catastrophe. As NACE International CEO Bob Chalker states: *"Whether it is a pipeline, an airplane, a water treatment plant or highway bridge, corrosion prevention and control is essential to avoiding catastrophic events before is too late"*.

In another study about corrosion in the United States, NACE estimates the annual cost of metallic corrosion to be 276 billion US\$. From this, the total direct cost in industrial categories was found to be 137,9 billion US\$ [5]. The study also classifies the costs into 5 main industry categories as it can be seen in Fig. 2.

**COST OF CORROSION IN INDUSTRY CATEGORIES
(\$137.9 BILLION)**

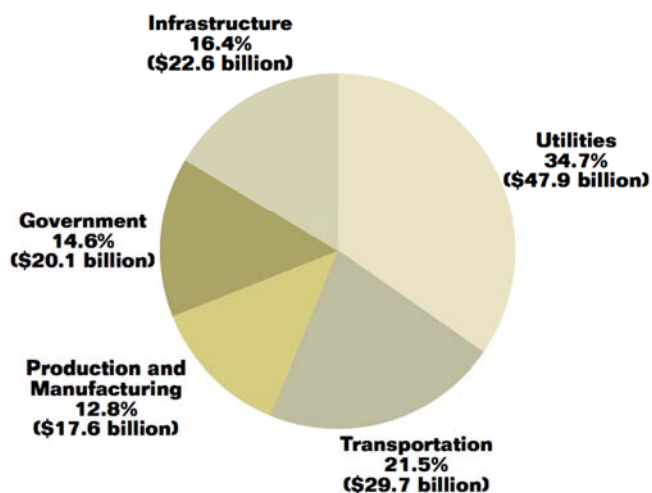


Fig. 2. Percentage and dollar contribution to the total cost of corrosion for the five sector categories analyzed [5].

INFRASTRUCTURE (\$22.6 BILLION)

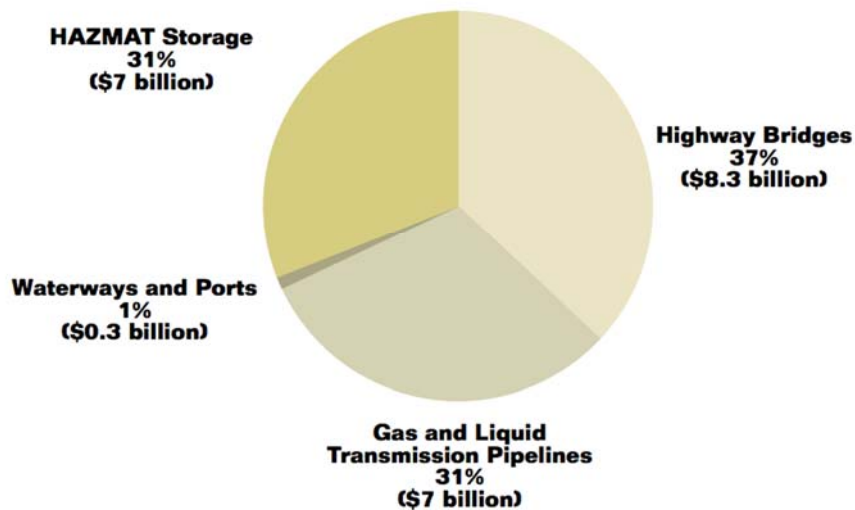


Fig. 3. Annual cost of corrosion in the infrastructure category [5].

UTILITIES (\$47.9 BILLION)

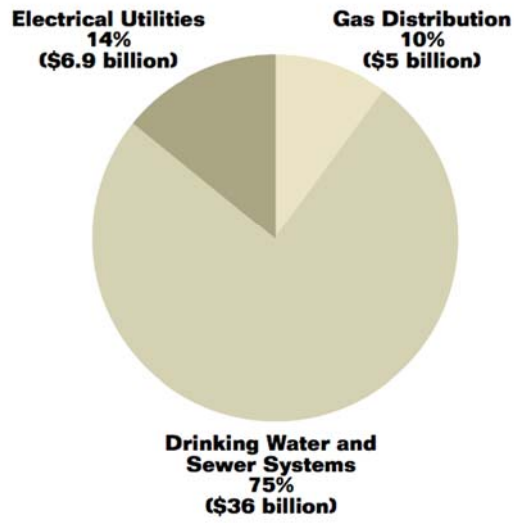


Fig. 4. Annual cost of corrosion in the utilities category [5].

TRANSPORTATION (\$29.7 BILLION)

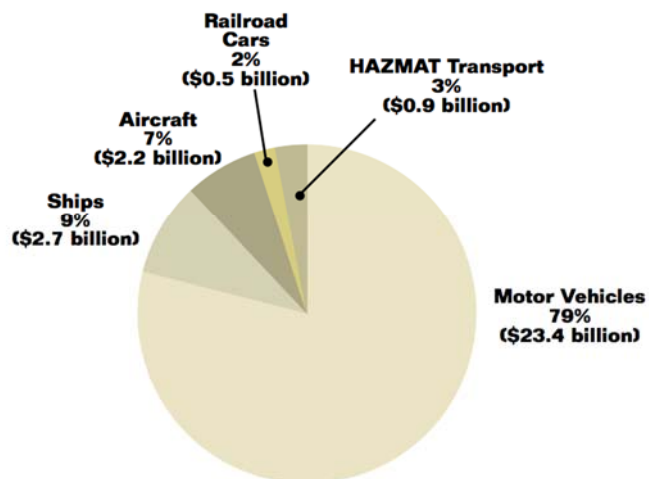


Fig. 5. Annual cost of corrosion in the transportation category [5].

PRODUCTION AND MANUFACTURING (\$17.6 BILLION)

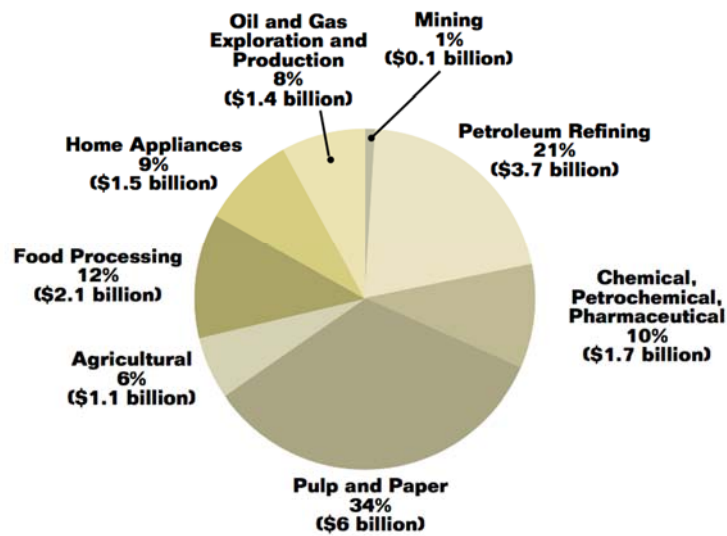


Fig. 6. Annual cost of corrosion in the production and manufacturing category [5].

2.3. Corrosion on aluminum, pitting corrosion

Although aluminum is a very reactive metal with a high affinity for oxygen, the metal shows a high corrosion resistance to most environments. This is due to the thin layer of aluminum oxide (Al_2O_3) that is formed on the surface of the metal. This passive layer, of around 5 to 10 nanometers thick, shows an inert and protective character and acts as a barrier between the metal and the surrounding medium [6]. As a consequence of this, aluminum and its alloys show a high resistance to uniform corrosion in most environments.

The main corrosion mechanism that affects aluminum is pitting corrosion. Pitting consists on localized attacks to the protective layer due to corrosive agents such as chlorides or acidic mediums. These attacks create cavities or holes of small size in the material, and the different types of pitting corrosion can be classified according to the shape of these pits, as shown in Fig. 7.

Trough Pits



Sideway Pits



Fig. 7. Different types of pitting corrosion [7].

These pits usually appear in mechanically damaged areas of the metal surface due for example to impacts, or in areas where there is a great quantity of chlorides or high acidity capable of breaking the protective layer.

Pitting corrosion is usually more dangerous than uniform corrosion because it is more difficult to predict, detect and act against. A small narrow pit can lead to the failure of an entire engineering system.

2.4. Anti-corrosion techniques

Anti-corrosion techniques are methods that aim for the protection of metallic surfaces from corrosive environments. There are a number of different anti-corrosion methods and sometimes two or more techniques can be applied together over the same surface. With these techniques it is possible to increase significantly the life of metallic components and reduce the corrosion-related costs.

Some of the common anti-corrosion techniques used for metallic surfaces are:

- **Galvanization:** It is mainly used in irons and steels. It consists on adding a layer of zinc (Zn) over the surface of the metal, which acts as a sacrificial protective layer. The reason for this is that in electrochemical corrosion the standard electrode potential (SEP) determines the ease by which the metal is oxidized or reduced. The lower the SEP is, the easier the metal is corroded. Fig. 8. shows the standard electrode potential of some elements. As Zn has lower SEP than iron, the metal that will be corroded will be zinc, thus protecting iron from corrosion. This technique is not used for aluminum substrates as Al has lower SEP than Zn.

Element	Electrode Reaction (Reaction)	Standard Reduction potential E° , volt
Li	$\text{Li}^{+} + e = \text{Li}$	-3.05
K	$\text{K}^{+} + e = \text{K}$	-2.925
Ca	$\text{Ca}^{+2} + 2e = \text{Ca}$	-2.87
Na	$\text{Na}^{+} + e = \text{Na}$	-2.714
Mg	$\text{Mg}^{+2} + 2e = \text{Mg}$	-2.37
Al	$\text{Al}^{+3} + 3e = \text{Al}$	-1.66
Zn	$\text{Zn}^{+2} + 2e = \text{Zn}$	-0.7628
Cr	$\text{Cr}^{+3} + 3e = \text{Cr}$	-0.74
Fe	$\text{Fe}^{+2} + 2e = \text{Fe}$	0.44
Cd	$\text{Cd}^{+2} + 2e = \text{Cd}$	-0.403
Ni	$\text{Ni}^{+2} + 2e = \text{Ni}$	0.25
Sn	$\text{Sn}^{+2} + 2e = \text{Sn}$	0.14
H_2	$2\text{H}^{+} + 2e = \text{H}_2$	+0.00
Cu	$\text{Cu}^{+2} + 2e = \text{Cu}$	+0.337
I_2	$\text{I}_2 + 2e = 2\text{I}$	+0.535
Ag	$\text{Ag}^{+} + e = \text{Ag}$	+0.799
Hg	$\text{Hg}^{+2} + 2e = \text{Hg}$	+0.885
Br_2	$\text{Br}_2 + 2e = 2\text{Br}$	+1.08
Cl_2	$\text{Cl}_2 + 2e = 2\text{Cl}$	+1.36
Au	$\text{Au}^{+3} + 3e = \text{Au}$	+1.50
F_2	$\text{F}_2 + 2e = 2\text{F}$	+2.87

Fig. 8. Standard electrode potential table.

- **Painting treatments on the surface:** Consist on the use of an anti-corrosive paint or powder coat on the metallic surface in order to avoid direct contact between corrosive compounds and the metal.
- **Surface treatments:** By chemical processes is possible to obtain a protective layer on the surface. Nitriding is an example of these surface treatments, and is mainly applied to steels.
- **Barrier coatings:** Consist on the use of coatings that act as a barrier and avoid the direct interaction between the metallic surface and the corrosive environment.

Covering the metal surface with a protective coating is an economic, effective and widely used method for reducing corrosion. Traditional coatings containing Cr and Pb have been prohibited by many countries because they are toxic for human health. This is why the development of ecofriendly polymeric coatings has gained special interest nowadays [8].

A technique that is increasing in popularity in the last few years is electrospinning, because it allows the deposition polymeric fibers over a metallic surface that can act as an effective barrier coating and reduce the corrosion of the metal.

2.5. Hydrophobicity, super-hydrophobic coatings

Hydrophobicity is basically the ability to repel water. The implementation of hydrophobic coatings can be used to increase the corrosion resistance of metallic substrates. This is because the electrochemical corrosion is a redox process that happens in an electrolyte medium, for example corrosion caused by chlorides in an aqueous solution. If the metallic surface presents a hydrophobic character there is less contact area between the metal and the electrolyte (water, aqueous solution), therefore less amount of aggressive ions have access to the metallic surface and corrosion rate is reduced.

Superhydrophobic coatings (SHCs) are those that exhibit a water contact angle (WCA) higher than 150° . These SHCs are used to lower the corrosion rate of Al and AAs in different aggressive environments and they have triggered quite attention in the last years due to their high water repelling properties.

Superhydrophobicity depends mainly on two surface parameters: the surface free energy and the surface roughness [9]. Superhydrophobic surfaces can be produced by increasing the roughness of the surface for the target material. Different techniques can be applied to produce rough surfaces. Some of these techniques are: chemical etching method [10], electrochemical deposition [11], sol-gel process [12] and layer-by-layer assembly [13].

Electrospinning is a powerful technique to synthesize ultrafine polymeric fibers, and the fiber film obtained has a high surface roughness providing hydrophobic or even superhydrophobic character [14].

The effect that surface roughness has on superhydrophobicity can be explained by the Cassie-Baxter wetting model [15], which attributes the surface superhydrophobicity to the air trapped underneath the liquid inside the interstices of this rough surface. This trapped air inhibits the electrolyte from penetrating to the metal surface, thus reducing the area of the redox reaction and therefore decreasing the corrosion rate.

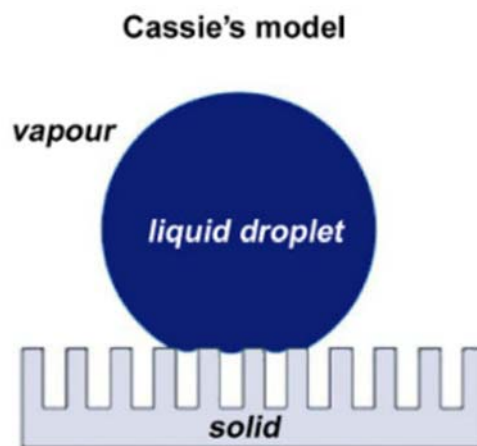


Fig. 9. Schematic of the Cassie-Baxter wetting model. As it can be seen, the trapped air prevents the liquid from penetrating to the solid surface.

CHAPTER 3: ELECTROSPINNING TECHNIQUE

3. ELECTROSPINNING TECHNIQUE

3.1. Fundamentals

The electrospinning technique consists basically on the utilization of electrostatic forces to generate polymer fibers. A typical electrospinning setup consists of a capillary through which the liquid (polymer solution) to be electrospun is forced, a high voltage source responsible for injecting charge into the liquid and a grounded collector (Fig. 10).

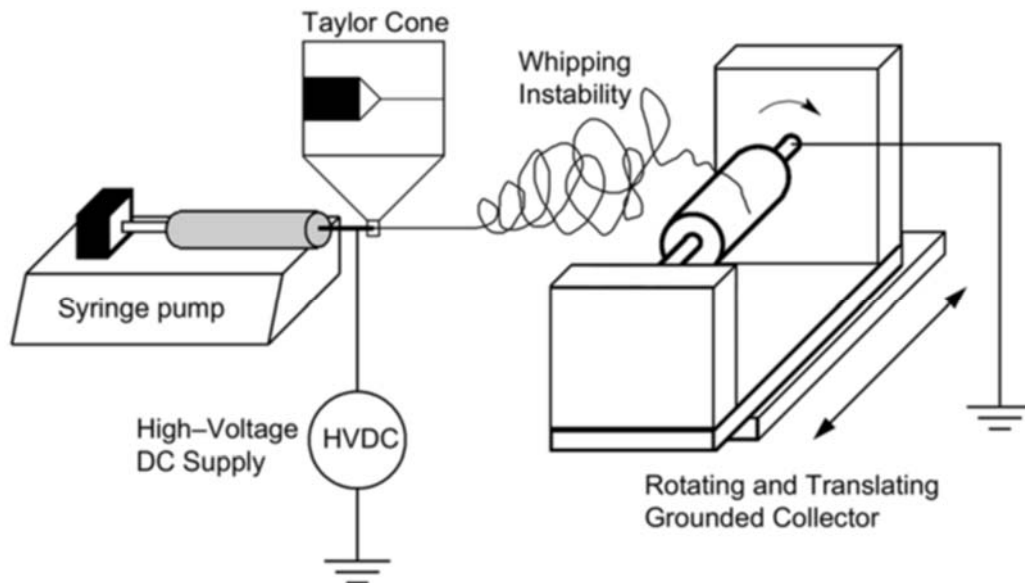


Fig. 10. Schematic of a typical electrospun setup [16].

As it can be seen in Fig. 10., a syringe pump is used to force the liquid through a small diameter capillary (needle), and a pendant drop is formed at the tip. Gravitational forces or pressurized gas are also alternative ways to force the liquid. The metallic needle is connected to a high voltage DC supply, which injects charge into the polymer solution. This charge can have positive or negative polarity.

By increasing the electric field strength tensile forces begin to appear on the liquid due to the repulsive forces between charges of the same polarity in the liquid and the attractive forces between the oppositely charged liquid and collector. If the electrostatic repulsive force between similar charges is high enough to overcome the surface tension of the liquid the Taylor cone is formed and a fiber jet is emitted from its apex and accelerated towards the grounded collector.

The travel of the fiber jet from the Taylor cone towards the collector is not straight and stable: while this jet flows through the atmosphere it undergoes a chaotic instability, bending in different directions and thereby increasing the travel time and the path length to the collector. This leads to fiber thinning because the solvent evaporation processes last longer [17].

Then the solid polymer fibers are deposited onto the grounded collector. This collector can be stationary, translating and rotating (as in Fig. 10.), or it can even be a solvent (e.g. water) depending on the application. If a stationary collector is used then randomly oriented fibers will be obtained, while the use of a rotary collector leads to the generation of aligned fibers.

3.2. Electrospinning parameters

There are different parameters that characterize the electrospinning process. These parameters must be optimized in order to generate fibers with the desired fiber properties. Recently, a greater understanding of the electrospinning parameters has led to the formation of very thin fibers, with diameters in the range of 100-500 nm, called nanofibers. The ability to produce nanofibers has increased the interest on the electrospinning technique in the last few years.

The different parameters can be classified as processing parameters (those that refer to the electrospinning technique itself) and solution parameters (those that refer to the properties of the polymer solution to be electrospun).

3.2.1. Processing parameters

3.2.1.1. Applied voltage

The strength of the applied electric field plays a huge role in the diameter of the generated fibers. Depending on the applied voltage it is possible to obtain fibers with diameter from several microns to tens of nanometers.

It also affects the shape of the surface at which the Taylor cone and the fiber jet are formed. With low applied voltages the Taylor cone forms at the tip of the pendant drop, but as the applied voltage increases the volume of the drop decreases and finally the Taylor cone is formed at the tip of the capillary [18].

There is an optimal range of applied voltage for a certain polymer/solvent electrospinning system. If the electric field is too weak or too strong this will lead to the formation of beaded fibers with undesired properties.

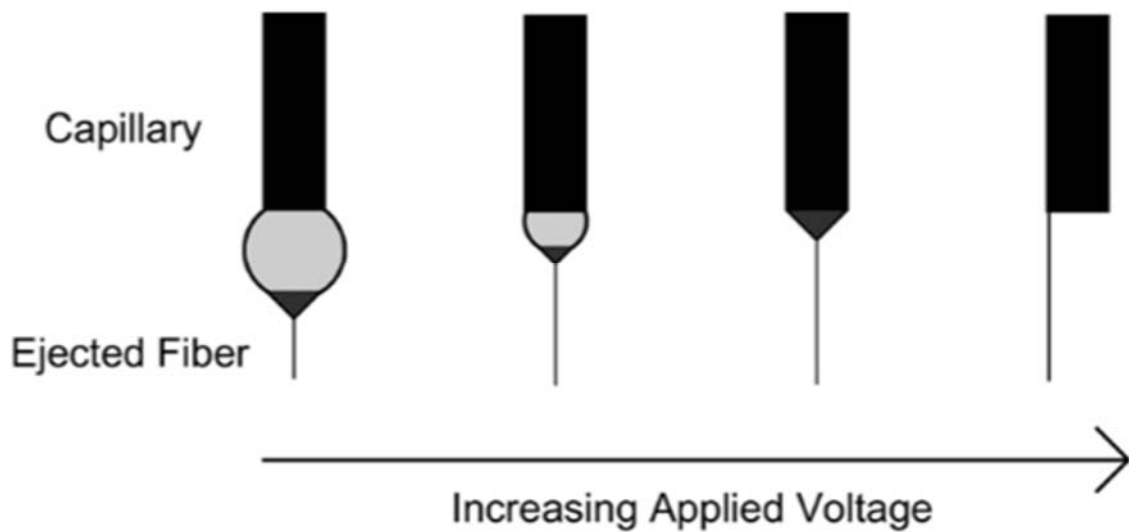


Fig. 11. Effect of varying the applied voltage on the formation of the Taylor cone [16].

3.2.1.2. Flow rate

The liquid flow rate also has a huge impact on fiber size, and it can also affect fiber porosity and fiber shape. The flow rate of the solution must be high enough in order to replace the solution ejected as a fiber jet.

Fiber diameter and pore size increase with increasing flow rate, and at very high flow rates beaded fibers are obtained due to the inability of fibers to dry completely before reaching the collector [19].

Therefore, there is also an optimal range for the solution flow rate for a certain polymer/solvent system. It must be high enough to allow a continuous jet formation but not so high for preventing bead defects.

3.2.1.3. Distance between capillary and collector

The distance between the capillary tip and the collector can also influence fiber size, but it plays a much smaller role than the applied voltage or the flow rate. Fiber diameter decreases as this distance increases [20].

Additionally, shortening the distance between the capillary and the collector below certain limits leads to the formation of beaded fibers and bead defects. This can also be due to an inadequate drying of the polymer jet [19].

3.2.2. Solution parameters

3.2.2.1. Polymer concentration

The polymer concentration determines whether the solution can be electrospun or not. It cannot be either too dilute or too concentrated. The polymer concentration affects the viscosity and the surface tension of the solution. If it is too dilute then the polymer fiber jet will break and droplets will be obtained instead of fibers. On the other hand, if the solution is too concentrated then fibers cannot be formed due to the high viscosity and the electrospinning is not possible.

There is an optimum range of polymer concentrations for each polymer in which fiber can be electrospun. Within this optimal range fiber diameter tends to increase with increasing polymer concentration [19].

3.2.2.2. Solvent volatility

For the electrospinning solution a volatile solvent must be used because solvent evaporation has to occur as the fiber jet travels through the atmosphere between the capillary tip and the collector. Some volatile solvents typically used for electrospinning are tetrahydrofuran (THF), dimethylformamide (DMF) or dimethylacetamide (DMAc).

3.2.2.3. Solution conductivity

Highly conductive solutions present a greater charge carrying capacity so the fiber jet will be subjected to a greater tensile force in the presence of an electric field than in solutions with lower conductivity. Baumgarten found that the radius of the fiber jet is inversely related to the cube root of the solution conductivity [21].

However this parameter plays a lesser role than other ones such as polymer concentration.

Parameter	Effect on fiber morphology
Applied voltage ↑	Fiber diameter ↓ initially, then ↑ (not monotonic)
Flow rate ↑	Fiber diameter ↑ (beaded morphologies occur if the flow rate is too high)
Distance between capillary and collector ↑	Fiber diameter ↓ (beaded morphologies occur if the distance between the capillary and collector is too short)
Polymer concentration (viscosity) ↑	Fiber diameter ↑ (within optimal range)
Solution conductivity ↑	Fiber diameter ↓ (broad diameter distribution)
Solvent volatility ↑	Fibers exhibit microtexture (pores on their surfaces, which increase surface area)

Table 1. Effects of electrospinning parameters on fiber morphology [16]. It is important to realize that these are general relationships; the exact effect will differ for each polymer/solvent system.

3.3. Why electrospinning?

In recent years the electrospinning technique has gained special interest as a potential polymer processing method due to its relative ease of use and the ability to fabricate fibers with diameter on the nanometer size scale. As it is a novel technique, further studies about the effect of the electrospinning parameters will help to understand better the process and to fabricate fibers with the desired morphology and properties.

For this work the electrospinning technique is chosen because it allows the deposition of polymer micro/nanofibers over a metallic substrate, in this case an aluminum alloy, obtaining a coating that acts as a barrier and presents a surface roughness high enough to provide a hydrophobic behaviour, thus decreasing the corrosion rate of the metal.

CHAPTER 4: MATERIAL SELECTION

4. MATERIAL SELECTION

4.1. Polymer selection: PS and PVC

A broad number of different polymers have been successfully electrospun; most of them are thermoplastics like polyaniline (PANI), polymethyl methacrylate (PMMA), polyvinylidene fluoride (PVDF), polystyrene (PS), polyacrylic acid (PAA), polyethylene oxide (PEO) or polyvinyl chloride (PVC) among others.

Polymer selection must be done in accordance with the future application and the desired properties for the resultant fiber structure. When aiming for improving the corrosion resistance not only is important to produce a fiber mat that covers the metal and acts as a barrier between the metallic surface and the corrosive environment, but also to increase the hydrophobic behaviour of the substrate. As the goal of this work is to obtain an anti-corrosion coating for an aluminum alloy, it is important to see which are the main types of corrosive environments that this metal will face.

Al and its alloys (AAs) present a high corrosion resistance to most environments due to the passive layer of Al_2O_3 formed at the surface, but they can suffer special damage from localized corrosion and pitting when they face an environment with high amount of corrosive compounds such as chlorides. These are mostly present in aqueous solution, and the specific substrate studied in this work, the aluminum alloy 6061T6, is used in applications that commonly encounter this aqueous corrosive media, like for example aircraft and marine components or dock structures.

If polymers soluble in water were to be used for the electrospinning of the coating fibers these fibers would dissolve in water once they faced the corrosive aqueous solution and therefore they would not be able to protect the metal from corrosion. In such case, a further treatment of the electrospun fibers would be necessary in order to increase the water repellency of the fiber mat. For example, polyacrylic acid (PAA) is a polymer with hydrophilic behaviour and the fibers of PAA obtained by electrospinning dissolve in water. To avoid this, a cross-linker agent such as β -cyclodextrin (β -CD) can be added to the polymeric solution prior to the electrospinning process in order to increase the water resistance [22]. The downside of this is that adding β -CD also increase the hydrophilic character, so further treatment would be needed for obtaining a hydrophobic structure.

It is possible to obtain directly electrospun fibers with water repellence properties if the polymer employed presents a hydrophobic character by nature. In the present work two different polymers are proposed: polystyrene (PS) and polyvinyl chloride (PVC). Both of them have hydrophobic nature and can be electrospun if they are dissolved in special solvents, as they are not soluble in water. A comparative study of the fibers obtained using separately PVC and PS will be performed in order to determine which polymer exhibits better anticorrosion properties.

4.2. Required solvents

As PVC and PS are not soluble in water, special solvents need to be used when preparing the polymeric solution prior to the electrospinning process. Solvents can be classified into two categories: polar and non-polar. Polar solvents are those substances that exhibit a permanent electric dipole due to the asymmetry in the distribution of their electron cloud. They generally present a dielectric constant greater than 15 [23] and they can be further divided into protic and aprotic.

Protic solvents are those with hydrogen bonds of the type O-H or N-H [24]. Water, ethanol and acetic acid are polar protic solvents. In the other hand, aprotic solvents are those without bonds O-H nor N-H. This type of solvent does not release protons in solution. Acetone, dimethylformamide (DMF), dimethylacetamide (DMAc) and tetrahydrofuran (THF) are examples of polar aprotic solvents.

Polyvinyl chloride and polystyrene are not soluble in water or other protic solvents therefore polar aprotic solvents must be used. These can also be classified into low boiling point solvents, such as acetone and THF; and high boiling point solvents, such as DMF and DMAc [25].

Initially for this work a single solvent system using tetrahydrofuran was chosen because a sample of THF was already available in the laboratories of the university, but the electrospinning process of PVC and PS was often interrupted by needle clogging and fibers could not be successfully electrospun. This phenomenon was attributed to the low boiling point of THF (66 °C) that produced the fast evaporation of the solvent at the exit of the capillary tip. Due to this, a binary solvent system consisting of DMF/THF was used. Both are polar aprotic solvents and the high boiling point of DMF (153 °C) can compensate the fast evaporation of THF.

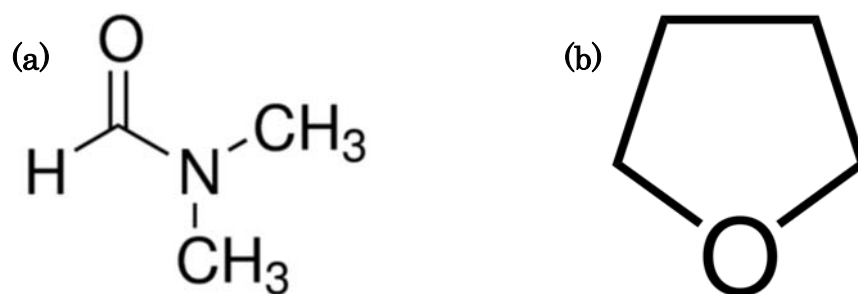


Fig. 12. Chemical structure of (a) DMF and (b) THF.

4.3. Metal oxide nanoparticles, ZnO

Corrosion resistance can be further enhanced by the addition of a corrosion inhibitor, either organic or inorganic. Many researchers have focused on blending a polymer with inorganic nanoparticles, such as Al₂O₃, ZrO₂, SiO₂, TiO₂, Fe₃O₄, CdS, and ZnO [9]. The presence of these nanoparticles between the interstices of the fibers can increase the surface roughness and the air entrapment, improving the hydrophobic character of the coating (following the Cassie-Baxter wetting model) and thus reducing the corrosion rate.

The main advantage of the electrospinning technique regarding to this metal oxide addition is that it produces a better distribution of the nanoparticles in the coating compared to other techniques like spray coating, and without using any dispersing agent [26]. Furthermore, the solution containing the blend of polymer plus inorganic nanoparticles can be prepared in one step only, which is another advantage of the electrospinning method.

For this work, the inorganic corrosion inhibitor employed will be ZnO. There are previous studies regarding the electrospinning of ZnO with polyvinylidene fluoride (PVDF) [9], polyvinyl alcohol (PVA) [27] or Nylon 6 [28]; but the corrosion behaviour of electrospun PVC-ZnO and PS-ZnO, to the best of our knowledge, has not been addressed previously.

4.4. List of purchased reagents

Polyvinyl chloride (PVC, $(C_2H_3Cl)_n$, $M_w = 80\ 000\ g/mol$), polystyrene (PS, $(C_8H_8)_n$, $M_w = 280\ 000\ g/mol$), and dimethylformamide (DMF) were purchased from Sigma-Aldrich.

Tetrahydrofuran (THF) and zinc oxide (ZnO) nanoparticles were already available in the laboratories of the Public University of Navarre (UPNA).



Fig. 13. Reagents employed, from left to right: ZnO, PS, PVC, DMF and THF.



Fig.14. ZnO nanoparticles in colloidal dispersion, 50% in H_2O . Average particle size of 50 nm.

CHAPTER 5: EXPERIMENTAL PROCEDURE

5. EXPERIMENTAL PROCEDURE

5.1. Optimization of the electrospinning parameters

The first step of the experimental procedure is to optimize the electrospinning parameters, mainly applied voltage (E) and flow rate (\dot{V}). The ultimate goal is to find the optimal values of those parameters that maximize the water repellency ability of the electrospun film, in order to increase the corrosion resistance of the final coating.

Ma et al. found that hydrophobicity generally increased with a reduction in fiber diameter [29], while Asmatulu et al. studied specifically the influence that fiber diameter has over the water contact angle (WCA) of PVC and PS electrospun fibers [30] and found that while for PS the WCA decreased linearly with fiber diameters bigger than 1 μm , in the case of PVC the WCA is almost constant and around 145° independently of fiber diameter in the range of 0-3 μm .

For this work, the optimization process can be divided in three steps: preparation of the polymer solution prior to the electrospinning process, electrospinning and fiber deposition of the samples varying the working parameters, and fiber characterization with WCA and fiber diameter measurements.

5.1.1. Polymer solution preparation

The solutions of PVC and PS will be separately prepared using the same binary solvent system consisting on DMF/THF, with a volume ratio 1:1 (that is same volume for both of the solvents). Initially a single solvent system using only THF was tried, but its low boiling point led to the fast evaporation of the solution at the end of the capillary tip, impeding the correct electrospinning of the fibers. The combined solvent provided the necessary volatility and conductivity required for the electrospinning solution.

An important parameter regarding the solution preparation is the polymer concentration. If the solution is too dilute the fiber jet will break without reaching the collector, and if it is too concentrated the high viscosity will difficult the process. Typically polymer concentrations between 10 wt% and 20 wt% are employed. In this work, a fixed concentration of 15 wt% is used.

The density of DMF is 0.944 g/ml and the density of THF is 0.889 g/ml. As the volume ratio for the solvent DMF/THF is 1:1, its resultant density is equal to:

$$\rho_{\text{solvent}} = \frac{\rho_{\text{DMF}} + \rho_{\text{THF}}}{2} = 0,9165 \text{ g/ml}$$

In order to obtain a polymer concentration of 15 wt%, 3.2 g of PVC and 3.2 g of PS were separately dissolved in a mixture of 10 ml of DMF and 10 ml of THF (1:1 ratio).

$$wt\% = \frac{3,2 \text{ g polymer}}{3,2 \text{ g polymer} + 20 * 0,9165 \text{ g solvent}} \times 100 = 14,86\%$$

The solutions were prepared under vigorous stirring (600rpm) for 12 hours at room temperature using a magnetic stirrer.



Fig. 15. Magnetic stirrer employed for the solution preparation.

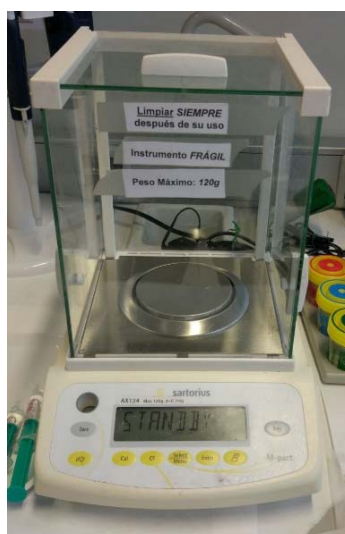


Fig. 16. Digital precision scale used to measure the polymer mass.

5.1.2. Fiber deposition at different applied voltages and flow rates

Several samples of both PVC and PS were electrospun with different electrospinning parameters, varying the voltage applied and the flow rate. These two are the processing parameters that have a bigger impact on the final morphology of the resultant fibers. The distance between the capillary tip and the collector was kept constant and equal to 15 cm in all the depositions, as this parameter plays a much smaller role than the other ones.

The electrospinning process was carried out using the Nadetech electrospinning equipment (Fig.17), which integrates the high voltage DC source, the syringe pump and the collector, which can be rotatory or fixed. A rotary collector allows to produce aligned fibers, but for this work a fixed aluminum collector was used because the heterogeneity of the fiber structure obtained with the fixed one improves the air entrapment capacity of the polymeric film, thus increasing the water repellency ability according to the Cassie-Baxter wetting model.



Fig. 17. Nadetech electrospinning equipment

The different samples were deposited onto standard microscope glass slides as the following fiber morphology characterization techniques, fiber diameter and WCA measurements; do not need to be carried out on the final aluminum substrate.

Firstly, the lower and upper limit values of the applied electric potential (E) and the flow rate (\dot{V}) that can be applied for each polymer need to be determined. In the case of PVC voltage values of 6 kV and lower showed to be too low and no fibers were deposited, whereas in the case of PS it was not possible to deposit fibers with voltage values equal to 9 kV and lower. There is also an upper limit for E above which the Taylor cone is no longer formed and the fiber jet is ejected from within the needle, which is associated with an increase in fiber defects [16]. For PVC the Taylor cone was observed to be formed in the range of 8-14 kV, whereas for PS the Taylor cone was formed in the range 11-17 kV. These values were chosen to be the lower and upper limits of the applied voltage for the set of experiments of the parameter optimization process.

Several samples of fiber mats were electrospun within the electrical potential range previously determined and at different flow rates, in order to study the effects these parameters have over the morphological characteristics of the obtained fibers.

5.1.3. Fiber characterization

5.1.3.1. Fiber diameter measurements

An optical microscope and the OLYMPUS Stream image analysis software were used to observe the morphology of the fibers and to measure the average fiber diameter of the different electrospun samples. Eight samples were produced and analyzed for each polymer, and the different solution and electrospinning parameters of each sample are shown in table 2.

SOLUTION DATA				ELECTROSPINNING PARAMETERS			
Sample	Polymer	Solvent	wt%	Voltage (kV)	Capillary-collector distance (cm)	Flow-rate (ml/h)	Deposition time (min)
A	PVC	DMF/THF (1:1)	15	12	15	1,2	20
B	PVC	DMF/THF (1:1)	15	12	15	0,8	20
C	PVC	DMF/THF (1:1)	15	12	15	1,0	20
D	PVC	DMF/THF (1:1)	15	12	15	0,6	20
E	PVC	DMF/THF (1:1)	15	10	15	0,8	20
F	PVC	DMF/THF (1:1)	15	8	15	0,8	20
G	PVC	DMF/THF (1:1)	15	6	15	0,8	NO FIBERS DEPOSITED
H	PVC	DMF/THF (1:1)	15	14	15	0,8	20
K	PS	DMF/THF (1:1)	15	15	15	1,5	12
L	PS	DMF/THF (1:1)	15	13	15	1,5	12
M	PS	DMF/THF (1:1)	15	11	15	1,5	12
N	PS	DMF/THF (1:1)	15	9	15	1,5	NO FIBERS DEPOSITED
Ñ	PS	DMF/THF (1:1)	15	17	15	1,5	12
O	PS	DMF/THF (1:1)	15	13	15	1,8	12
P	PS	DMF/THF (1:1)	15	13	15	0,9	12
Q	PS	DMF/THF (1:1)	15	13	15	1,2	12

Table 2. Solution and electrospinning parameters for the different samples produced for the parameter optimization process.

In order to determine the fiber diameter of each sample, 10 measurements were performed at different fibers in the same sample and then the arithmetic mean and standard deviation were computed. Results are shown in table 3.

	*All values in micrometers											
Sample	Measure 1	Measure 2	Measure 3	Measure 4	Measure 5	Measure 6	Measure 7	Measure 8	Measure 9	Measure 10	Mean	Standard Dev.
A	1,51	1,16	1,17	1,16	1,11	1,57	1,23	1,12	1,19	1,27	1,25	0,161
B	1,71	1,05	1,51	0,97	1,06	0,72	1,26	0,97	1,12	1,04	1,14	0,286
C	0,84	0,93	1,13	1,13	1,21	1,50	1,14	1,13	1,51	1,37	1,19	0,220
D	0,55	0,78	0,69	1,08	0,99	0,83	1,02	1,01	0,82	0,96	0,87	0,169
E	1,46	1,16	1,23	1,01	1,09	0,98	0,89	1,60	1,50	1,10	1,20	0,241
F	1,42	2,42	1,79	1,70	1,16	1,72	1,34	2,01	1,37	2,10	1,70	0,393
H	0,95	0,87	0,90	1,25	1,10	0,91	1,26	1,58	1,36	0,64	1,08	0,280
K	2,57	2,87	2,59	3,07	2,44	2,70	2,75	2,27	2,67	3,08	2,70	0,257
L	2,52	2,12	2,34	2,28	2,42	1,75	2,31	2,20	2,23	2,79	2,30	0,270
M	2,42	2,03	2,56	2,05	2,60	2,01	2,28	1,80	1,92	2,02	2,17	0,278
N	2,68	2,35	3,01	3,02	3,08	2,84	3,22	3,12	3,01	2,85	2,92	0,253
O	3,42	4,61	4,87	3,90	4,23	4,20	4,42	3,79	4,09	4,20	4,17	0,413
P	2,39	1,75	2,29	1,63	2,08	2,01	2,22	1,86	1,99	2,51	2,07	0,282
Q	2,76	2,47	2,16	2,46	2,34	2,42	2,39	1,92	2,39	2,60	2,39	0,228

Table 3. Fiber diameter measurements, arithmetic mean and standard deviation. Samples A-H correspond to PVC and samples K-Q correspond to PS. (Note that samples G and N are not present. These are the samples where no fibers were deposited due to very low voltage).

In general terms, it can be observed that PVC fibers are thinner than PS ones. PVC fiber diameters have values around 1 μm while PS fiber diameters have values in the range 2-4 μm .

In the case of PVC the thinnest fibers obtained, with a mean diameter equal to 0.87 μm , correspond to sample D, which is the one produced with the lowest flow rate between all PVC samples. Also in the case of PS the thinnest fibers obtained, with a mean diameter equal to 2.07 μm , correspond to sample P, which is the one produced with the lowest flow rate between all PS samples.

The thickest fibers of PVC showed a mean diameter of 1.70 μm , whereas the thickest fibers of PS presented a mean diameter of 4.17 μm .

The reason for the PS fibers being thicker than the PVC ones can be attributed to the higher viscosity of the PS solution. In both cases the polymer concentration was 15 wt%, and the solvent system was equal (DMF/THF with volume ratio 1:1), but the viscosities were not the same. This is because of the different molecular weight of the polymers: the PVC employed had a molecular weight $M_w = 80\ 000\ \text{g/mol}$ whereas the PS had a molecular weight $M_w = 280\ 000\ \text{g/mol}$.

Dreval' et al. studied the effect of molecular weight of polystyrene on the viscosity of concentrated solutions and found that solution viscosity increased with an increase in molecular weight [31]. In general, the relationship between viscosity and molecular weight can be described using the Mark-Houwink equation [32]:

$$\eta = K * M^a$$

This equation shows that intrinsic viscosity (η) is proportional to the molecular weight of the dissolved polymer (M), with K and a being constant parameters that depend on the solvent system. In this work, the solvent system used was the same for all samples, so the bigger molecular weight of polystyrene led to a more viscous solution, and therefore the PS fibers produced were thicker than the PCV ones.

Figures 18 and 19 are optic microscope images showing the fiber diameter measurements realized:

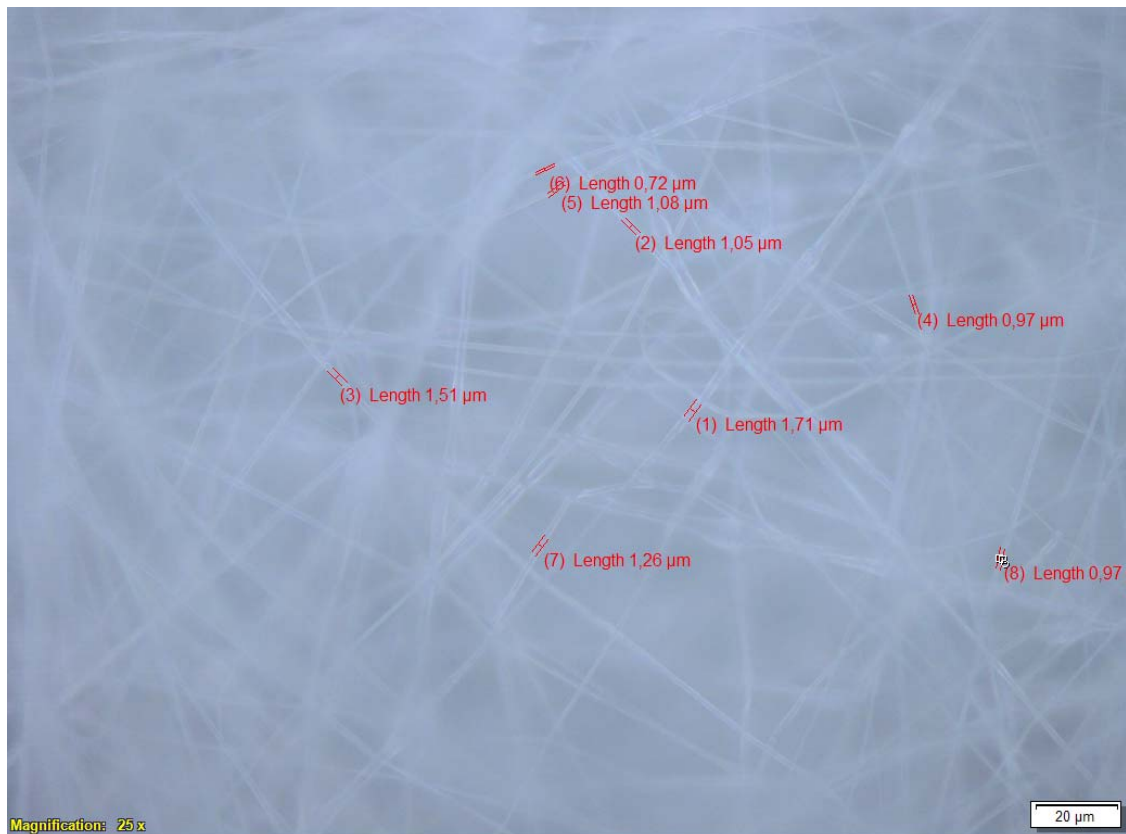


Fig. 18. Optical microscope image of PVC fibers corresponding to sample B, which were electrospun with a voltage of 12 kV and a flow rate of 0.8 ml/h.

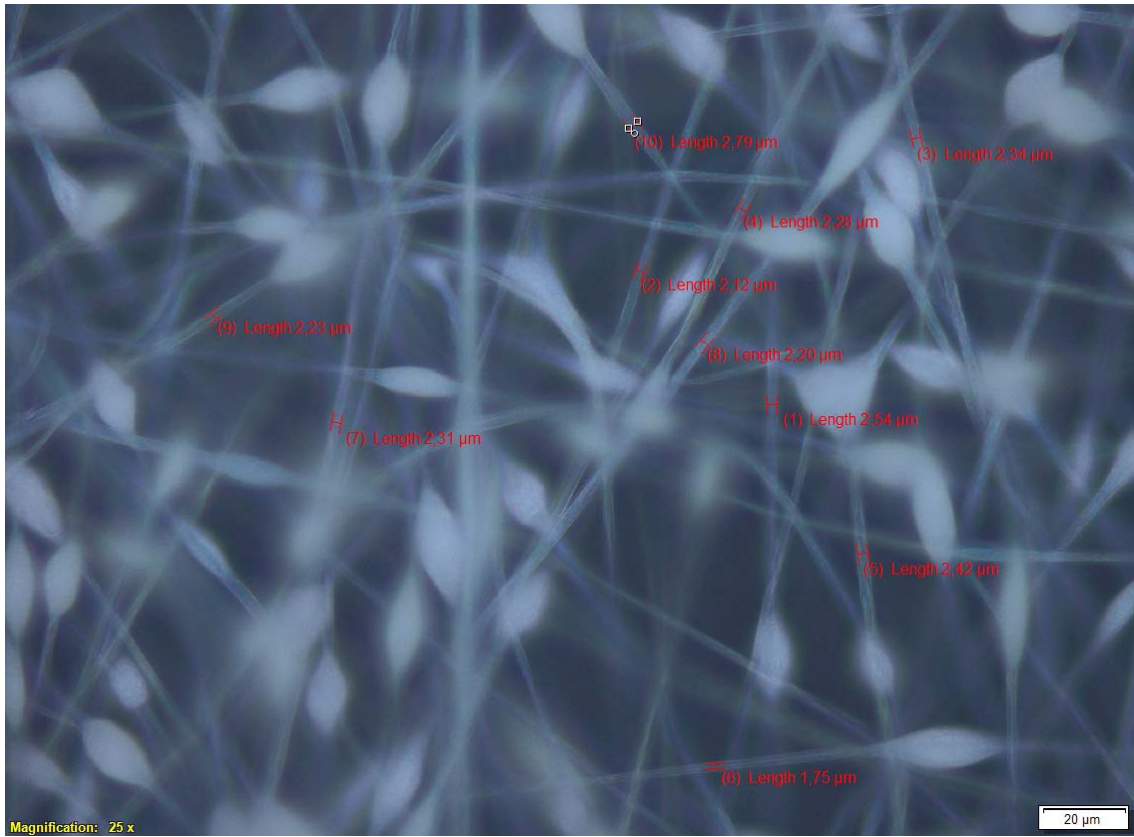


Fig. 19. Optical microscope image of PS fibers corresponding to sample L, which were electrospun with a voltage of 13 kV and a flow rate of 1.5 ml/h.

Another morphological feature that could be observed is higher amount of beads (those rounded polymer agglomerations) formed between the polystyrene fibers. This may also be attributed to the higher viscosity of the PS solution.



Fig. 20. Optical microscope employed for the fiber diameter measurements.

In order to determine the variation of the fiber diameter as a function of the flow rate four samples for each polymer were produced keeping a constant applied voltage and varying the flow rate in fixed intervals. In the case of PVC the voltage was kept constant and equal to 12 kV and four different samples were electrospun at 0.6, 0.8, 1.0 and 1.2 ml/h flow rates. For PS the applied voltage was fixed at 13 kV and the flow rate values were 0.9, 1.2, 1.5 and 1.8 ml/h. Results are shown in figures 21 and 22.

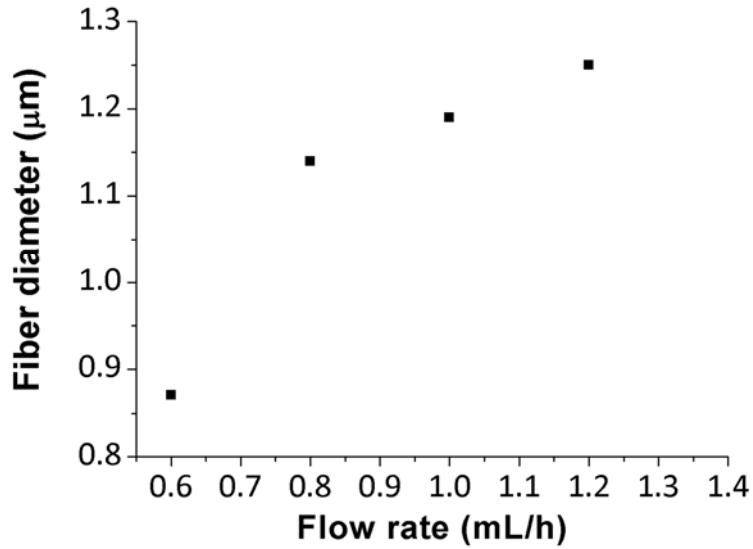


Fig. 21. Evolution of the fiber diameter as a function of the flow rate in the case of the PVC fibers. Fixed applied voltage of 12 kV.

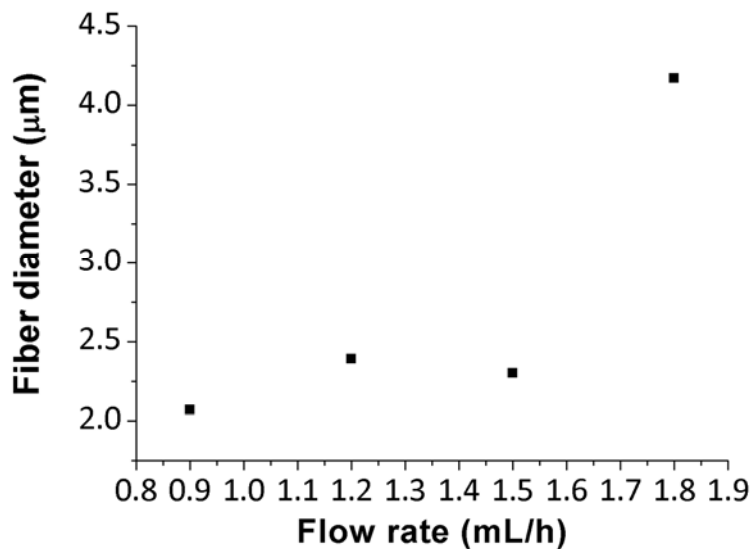


Fig. 22. Evolution of the fiber diameter as a function of the flow rate in the case of the PS fibers. Fixed applied voltage of 13 kV.

It can be clearly seen how the PVC fibers became thicker when increasing the flow rate, with a big jump when this last one is increased from 0.6 to 0.8 ml/h. The same tendency was observed with the PS fibers, they became thicker when increasing the applied flow rate. This cannot be well appreciated in Fig. 22. because the mean fiber diameter corresponding to a flow rate of 1.5 ml/h resulted lower than the one corresponding to 1.2 ml/h. The reason for this is because initially this increase in fiber diameter is small and the values represented in the graph are just the mean values, but their standard deviation is around 0.25 (exact standard deviation values can be seen in table 3), so these points corresponding to flow rates of 1.2 and 1.5 ml/h have very close mean values that fall in the range of the standard deviation. The increase of fiber diameter can be clearly observed when the flow rate is increased from 1.5 to 1.8 ml/h. Therefore for both polymers it is possible to affirm that fibers become thicker with bigger flow rate values, and this matches with literature [16, 19].

In order to determine the influence of applied voltage over the fiber diameter a similar procedure is held: four samples for each polymer were electrospun keeping a fixed flow rate and varying the applied voltage in fixed intervals. In the case of PVC the flow rate was kept constant and equal to 0.8 ml/h and the samples were produced at 8, 10, 12 and 14 kV; whereas in the case of PS the flow rate was fixed at 1.5 ml/h and the samples were electrospun at 11, 13, 15 and 17 kV. Results are shown in figures 23 and 24.

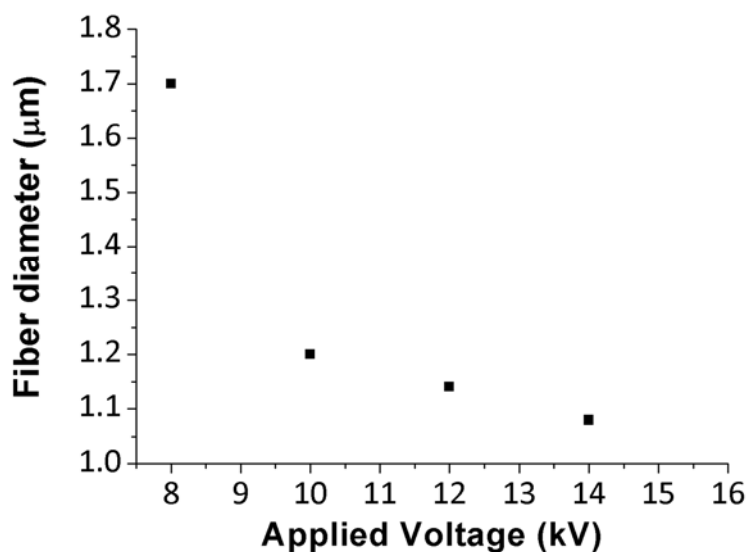


Fig. 23. Evolution of the fiber diameter as a function of the applied voltage in the case of the PVC fibers. Fixed flow rate of 0.8 ml/h.

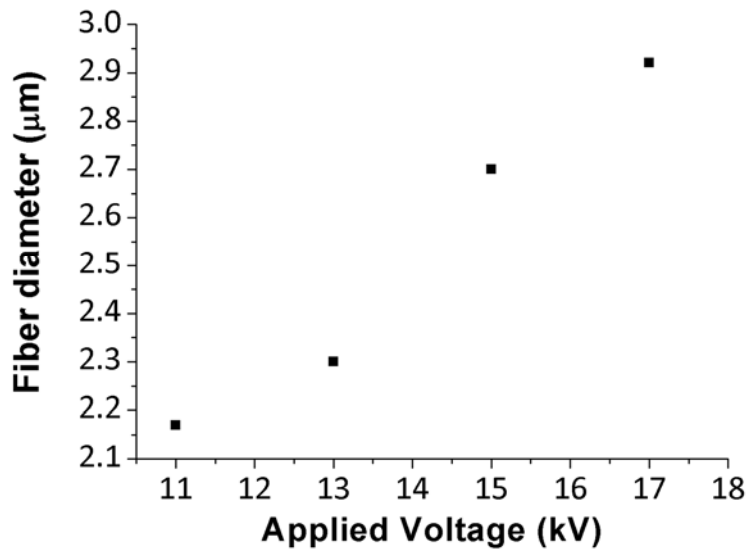


Fig. 24. Evolution of the fiber diameter as a function of the applied voltage in the case of the PS fibers. Fixed flow rate of 1,5 ml/h.

The influence applied voltage has on the resultant fiber diameter has not been perfectly defined yet. For example, Reneker and Chun [33] have demonstrated that there is not much effect of applied voltage on the diameter of electrospun polyethylene oxide (PEO) nanofibers. Some studies suggest that higher voltages facilitate the formation of large diameter fibers, like Bakar et al. who studied how Polyacrylonitrile (PAN) electrospun nanofibers increased their diameter with increasing applied voltages [34]. Others suggest that higher voltages can increase the electrostatic repulsive force on the charged jet, thus narrowing the fiber diameter, for example Yuan et al. [35] observed that polysulfone (PSF) electrospun fibers presented lower diameters when increasing the applied voltage. Therefore it can be concluded that voltage does influence fiber diameter but it can lead to different effects depending on the polymer employed.

These two different behaviours can be observed in the two polymers studied in this work. In the one hand, fiber diameter of PVC electrospun fibers decrease with increasing applied voltage, while in the other hand fiber diameter of PS electrospun fibers increase with increasing applied voltage. This last result matches the results obtained by Huan et al. who observed the effect of applied voltage over the morphological properties of PS fibers [36].

5.1.3.2. Water Contact Angle (WCA) measurements

The main goal of the optimization process is to find the electrospinning parameters that maximize the hydrophobicity or water repellency of the electrospun coatings. The WCA measurements provide information about the hydrophobic behaviour of the studied surface.

WCA measurement technique consists on depositing a single drop of pure water over the surface to be studied, and using a high-resolution camera and an image processing software it is possible to determine the angle between the water drop and the surface plane.

Low WCA ($<90^\circ$) are related to hydrophilic surfaces, while high WCA ($>90^\circ$) correspond to hydrophobic surfaces, being 180° the maximum contact angle attainable. Superhydrophobic surfaces are those that exhibit WCA higher than 150° and present excellent water repelling and self-cleaning properties.



Fig. 25. CAM 100 contact angle goniometer employed for the WCA measurements.

For the determination of the WCA, the same samples of the previous section (section 5.1.3.1. "*Fiber diameter measurements*") were analyzed. For each sample 5 WCA measurements were taken in 5 different zones, and then the arithmetic mean was computed. Figures 26 and 27 are examples of some WCA measurements.

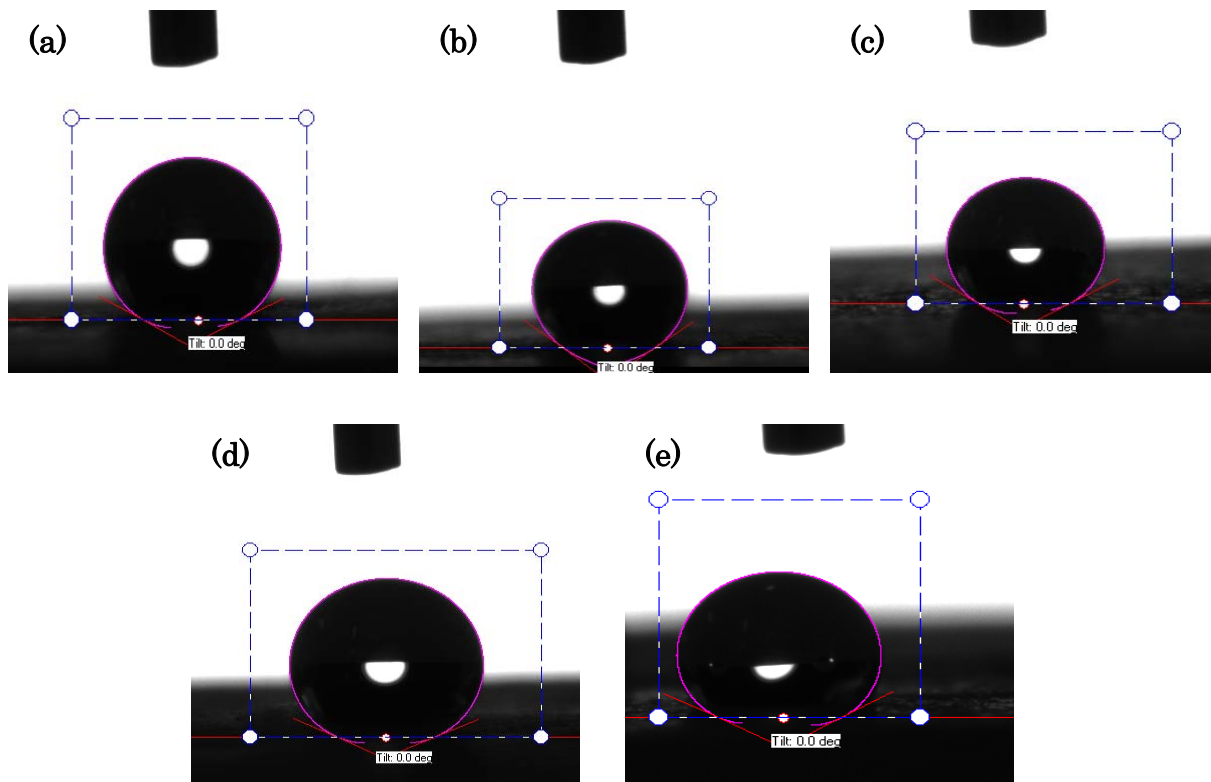


Fig. 26. Optical images of the water contact angle on sample H (PVC). The WCA measurements were (a) 151.73°, (b) 148.40°, (c) 151.66°, (d) 152.24° and (e) 150.91°; which lead to a mean value of WCA = $151 \pm 2^\circ$, highest among all PVC samples.

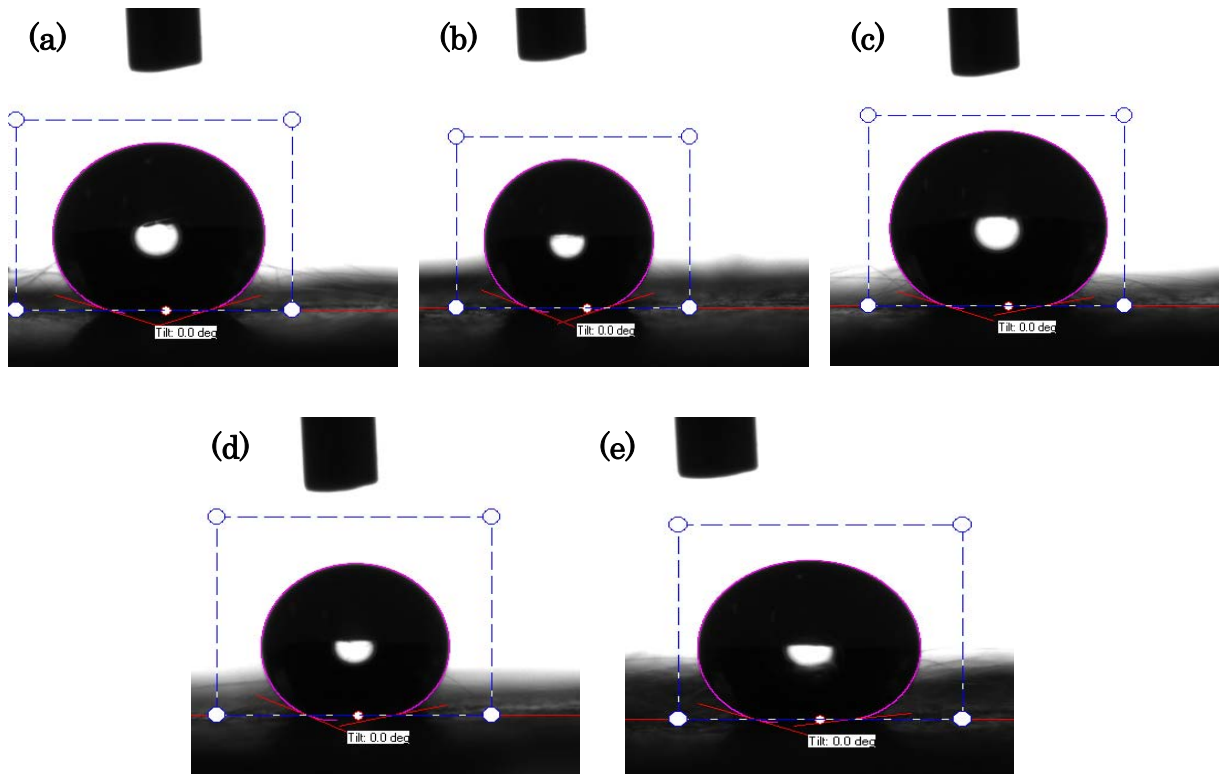


Fig. 27. Optical images of the water contact angle on sample P (PS). The WCA measurements were (a) 162.28°, (b) 159.97°, (c) 165.93°, (d) 161.69° and (e) 166.59°; which lead to a mean value of WCA = 163 ± 3°, highest among all PS samples.

The values of the mean WCA for all the samples are displayed in Table 4, along with the mean fiber diameter.

Polymer	Sample	FIBER PROPERTIES	
		Fiber diameter (μm)	Water CA (deg)
PVC	A	1,25	150
	B	1,14	143
	C	1,19	149
	D	0,87	144
	E	1,20	147
	F	1,70	143
	G	/	/
	H	1,08	151
PS	K	2,70	161
	L	2,30	159
	M	2,17	162
	N	/	/
	Ñ	2,92	161
	O	4,17	162
	P	2,07	163
	Q	2,39	159

Table 4. Fiber properties (Fiber diameter and WCA) results for all samples. *Note that the displayed results are mean values.

From these results some observations can be made: (1) PS samples present higher WCA than PVC ones, (2) the WCA of all PS samples is higher than 150° therefore they are considered superhydrophobic, (3) two samples of PVC (samples A and H) are superhydrophobic while the rest have WCA slightly lower than the 150° threshold, and (4) there is little variation in the WCA values: the results corresponding to PVC are within the range 143 to 151° whereas those corresponding to PS are within the range 159 to 163° .

Polystyrene fibers showed to have a very high water repelling behaviour, which was clearly noticeable during the WCA tests as it was quite difficult to deposit the water drop onto the sample surface because it was not immediately attached to it, even if little pressure was applied. This can be explained because of the high surface roughness of the PS coatings (higher than the PVC ones), which is enhanced by the greater amount of beads present. Such high surface roughness increases the air entrapment between the fibers, thus improving the water repellency of the coating (Cassie-Baxter wetting model).



Fig. 28. Picture of a water drop deposited on a surface coated with electrospun PVC fibers. The high water repellency and WCA can be observed at a glance.

Once fiber characterization tests have been performed it is possible to determine how the electrospinning parameters of applied voltage and flow rate should be established if a minimization of the fiber diameter is being pursued. Based on the trends observed in figures 21 to 24, and with the goal to produce thin fibers, a low flow rate and high voltage should be applied in the case of PVC, whereas a low flow rate and low voltage should be applied in the case of PS.

5.2. Corrosion inhibitor (ZnO) addition

Corrosion resistance can be further enhanced by the addition of a corrosion inhibitor. For this work, inorganic nanoparticles of ZnO will be incorporated to the polymeric film creating a composite structure that will theoretically improve the anti-corrosion properties of the coating. The role of ZnO in enhancing the corrosion resistance is related to decreasing the pore size of the composite film and increasing the air entrapment within the interstices of the surface [9].

The main advantage of the electrospinning technique is that the corrosion inhibitor incorporation can be made directly in one step by adding ZnO nanoparticles in the polymer solution prior to the electrospinning process.

This process can be divided in three steps: solution preparation, electrospinning of the nanocomposite fiber mat, and a final characterization process in order to ensure that ZnO has been added correctly into the sample.

5.2.1. Solution preparation

Firstly the polymer solutions were prepared as in section 5.1.1. ("*Polymer solution preparation*"), dissolving separately 3.2 g of PVC and 3.2 g of PS into a binary solvent system consisting of a mixture of 10 ml of DMF and 10 ml of THF; therefore obtaining PVC and PS solutions of polymer concentration 15 wt%. These solutions were prepared under vigorous stirring (600 rpm) for 12 h at room temperature using a magnetic stirrer.

Separately, 0.64 g of the zinc oxide colloidal dispersion (50% in H₂O) were added to a mixture of 1 ml of DMF and 1 ml of THF (same 1:1 solvent volume ratio as the polymer solution). As the zinc oxide colloidal dispersion has a ZnO content of 50 wt% in H₂O, 0.32 g out of the total of 0.64 g correspond to zinc oxide nanoparticles. The ZnO concentration in the binary solvent DMF/THF will be 15 wt% (disregarding the mass of water). Two samples of this ZnO mixture were produced and dispersed applying stirring (200 rpm) for 12 h at room temperature.

Finally the dispersed ZnO mixtures were added to the PVC and PS solutions, and then vigorous stirring (600 rpm) was again applied for 2 h in order to allow for an adequate mixing.

5.2.2. Electrospinning of the composite mixtures

The electrospinning of the fibers containing ZnO nanoparticles was carried out using the optimized electrospinning parameters from section 5.1. (*"Optimization of the electrospinning parameters"*). Conditions of highest applied voltage and lowest flow rate will be used for the electrospinning of the PVC fibers, therefore 14 kV and a flow rate of 0.6 ml/h will be applied. In the other hand, for the electrospinning of the PS fibers processing conditions of lowest applied voltage and lowest flow rate will be employed, that is 11 kV and a flow rate of 0.9 ml/h.

The distance between the capillary tip and the collector was kept constant and equal to 15 cm, and the deposition time was fixed at 10 minutes for all depositions.

The composite fiber films were deposited again onto standard microscope glass slides, as the fiber characterization tests that would be performed afterwards did not need to be carried out over the final aluminum substrate.

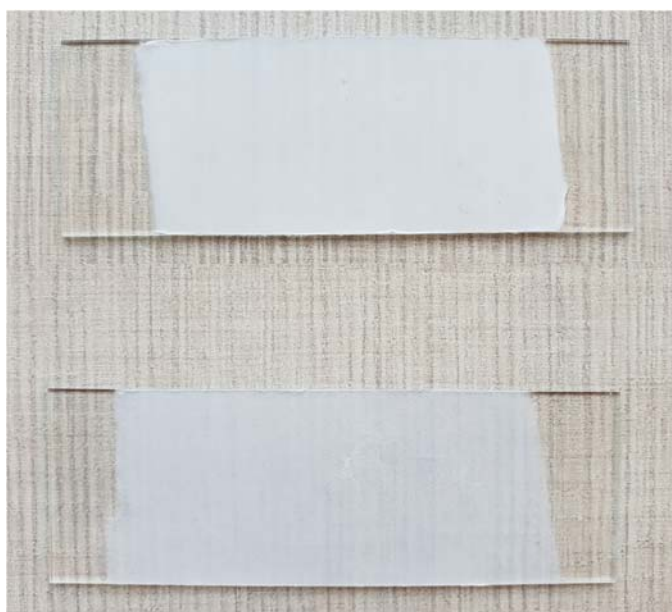


Fig. 29. Depositions of PVC+ZnO (top) and PS+ZnO (bottom) fibers onto standard microscope glass slides. The whiter color of the PVC film may be related to a higher density of polymer fibers.

5.2.3. Characterization of the polymer+ZnO fibers

After the composite coatings of PVC and PS with zinc oxide nanoparticles were correctly electrospun, several characterization techniques were employed with two different goals: (1) checking that the ZnO nanoparticles were correctly incorporated into the fiber mat and (2) checking that the use of the optimized electrospinning parameters led to the generation of thinner fibers with high WCA as expected.

For doing so, thermogravimetric analysis (TGA), fiber diameter measurements with an optical microscope and WCA measurements were performed.

5.2.3.1. Thermogravimetric analysis

Thermogravimetric analysis (TGA) is a method of thermal analysis in which the mass of a sample is measured over time as the temperature increases [37]. This technique can be used to determine the presence of ZnO nanoparticles in the electrospun coatings. As the temperature increases the polymer starts to decompose and finally all the mass of the sample will correspond to the metal oxide nanoparticles that have a much higher melting and evaporation points compared to those of the polymer.



Fig. 30. Thermogravimetric analyzer of the AIN (Asociación de la Industria Navarra), where the TGA tests were performed.

The results of the TGA tests carried out can be seen in figures 31 and 32:

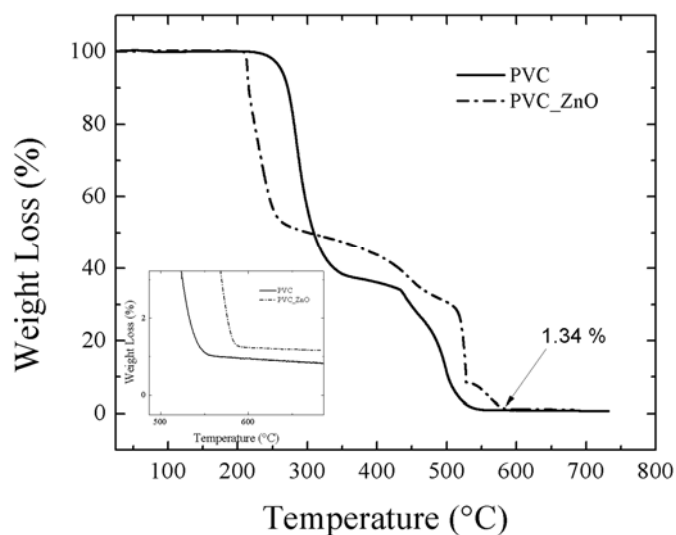


Fig. 31. Thermal gravimetric analysis (TGA) of both PVC fibers with no corrosion inhibitor (solid line) and PVC fibers containing zinc oxide nanoparticles (dash-dotted line).

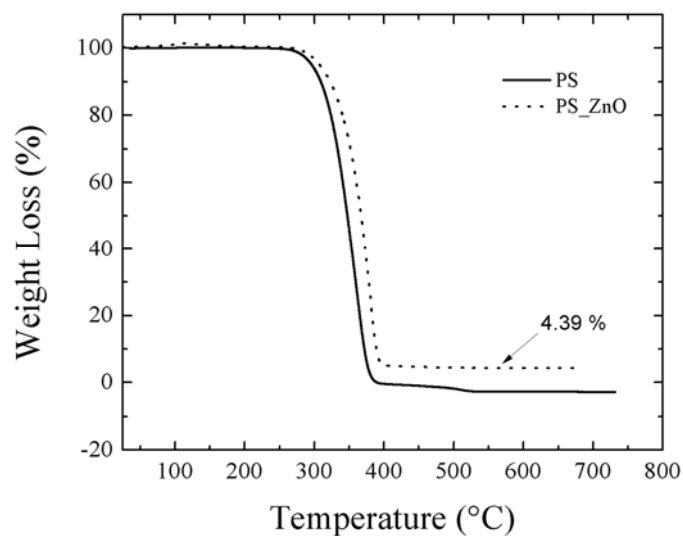


Fig. 32. Thermal gravimetric analysis (TGA) of both PS fibers with no corrosion inhibitor (solid line) and PS fibers containing zinc oxide nanoparticles (dotted line).

TGA tests confirmed the successful fabrication of nanocomposite fibers containing ZnO nanoparticles. However it could be observed that a bigger content of ZnO was present in the PS sample. The reason for this may be a better nanoparticle dispersion in the PS solution prior to the electrospinning process, or it may just be because the samples analyzed in the TGA tests are small and localized samples and not the whole fiber mat is tested, so if the distribution of ZnO particles is not uniform these localized differences could be observed.

5.2.3.2. Fiber diameter measurements

In order to check if the optimized electrospinning parameters led to the fabrication of thinner fibers, 10 measurements of fiber diameter were performed to both the PVC+ZnO and PS+ZnO samples using an optical microscope and the OLYMPUS Stream image analysis software. All the measurements with the computed arithmetic mean and standard deviations are displayed in table 5.

	*All values in micrometers											
Sample	Measure 1	M. 2	M. 3	M. 4	M. 5	M. 6	M. 7	M. 8	M. 9	M. 10	Mean	Standard Deviation
PVC+ZnO	0,57	0,76	0,67	0,67	0,60	0,97	0,67	0,85	0,67	0,81	0,72	0,123
PS+ZnO	2,20	1,82	2,15	1,62	2,24	1,93	2,71	2,05	2,16	2,08	2,10	0,288

Table 5. Fiber diameter measurements, arithmetic mean and standard deviations, for both PVC+ZnO and PS+ZnO composite fibers electrospun under the optimized processing parameters.

The fiber diameter measurements showed that the PVC nanocomposite fibers produced with the optimized electrospinning parameters presented diameter values in the nanometric range, with a mean value of 720 nm. This is the lowest fiber diameter mean value obtained among all the samples of this work.

On the other side, the mean diameter of the PS nanocomposite fibers was found to be 2.10 μm . This value goes into accordance with the observed trend regarding the evolution of the PS fiber diameter as a function of applied voltage and flow rate. With a low applied voltage (11 kV) fiber diameters have values close to 2 μm for flow rates in the range 0.9 to 1.5 ml/h, and with a higher flow rate like 1.8 ml/h a big increment in the fiber diameter is noticed.

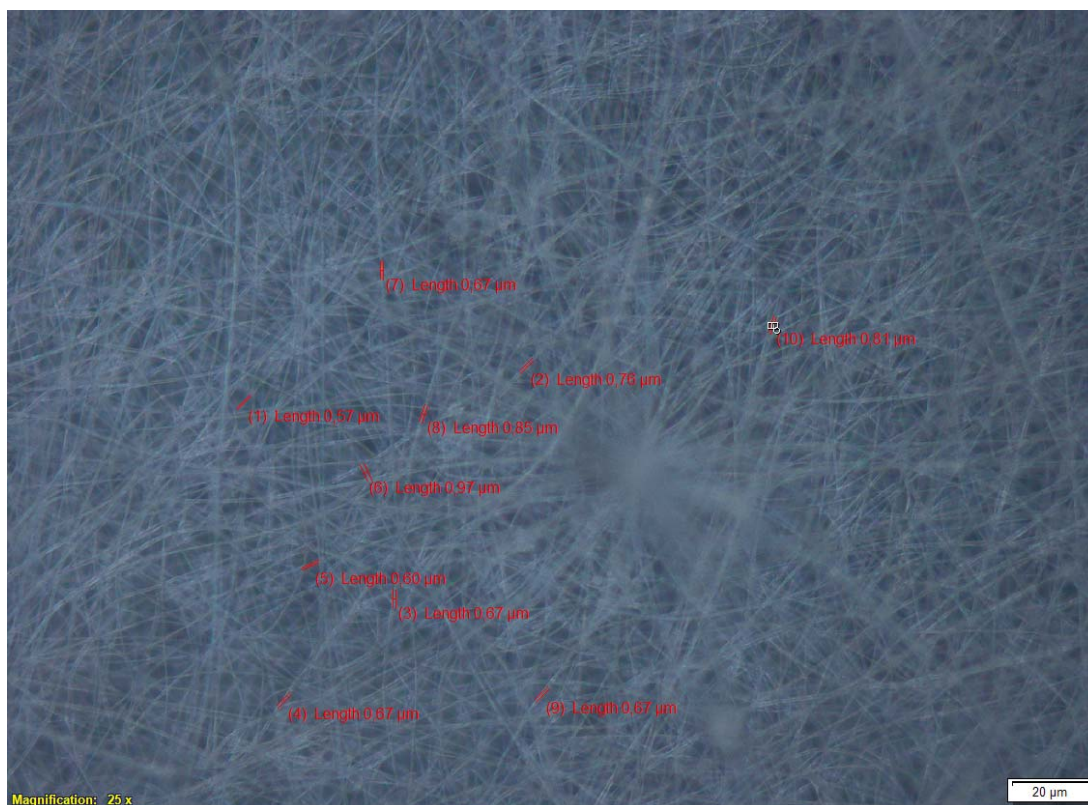


Fig. 33. Optical microscope image of PVC+ZnO fibers, electrospun with a voltage of 14 kV and a flow rate of 0.6 ml/h.

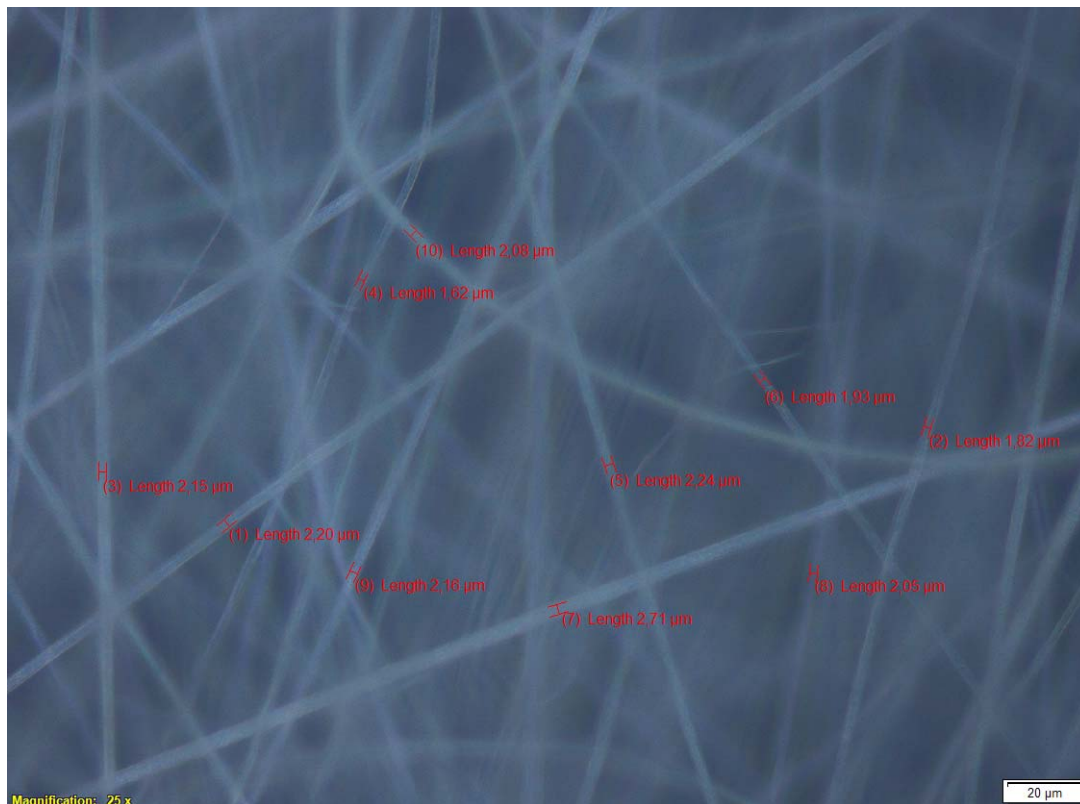


Fig. 34. Optical microscope image of PS+ZnO fibers, electrospun with a voltage of 11 kV and a flow rate of 0.9 ml/h.

Another observation that could be inferred from the optical microscope images is that the PVC samples present a higher fiber density than the PS ones, so this could explain the whiter color of the PVC coatings (see Fig. 29).

5.2.3.3. Water contact angle measurements

WCA tests were performed over the nanocomposite surfaces for both PVC+ZnO and PS+ZnO. In order to determine the WCA 3 measurements were taken in 3 different zones for each sample, and then the arithmetic mean was computed. All measurements were taken at room temperature. The results are shown in figures 35 and 36.

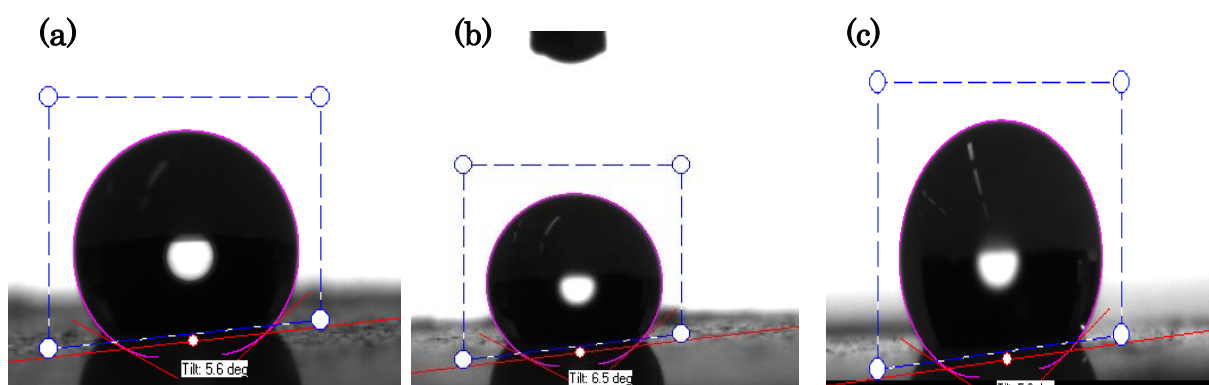


Fig. 35. Optical images of the water contact angle on the PVC+ZnO sample. The WCA measurements were (a) 146.39° , (b) 146.05° and (c) 148.88° , which lead to a mean value of $\text{WCA}=147 \pm 2^\circ$.

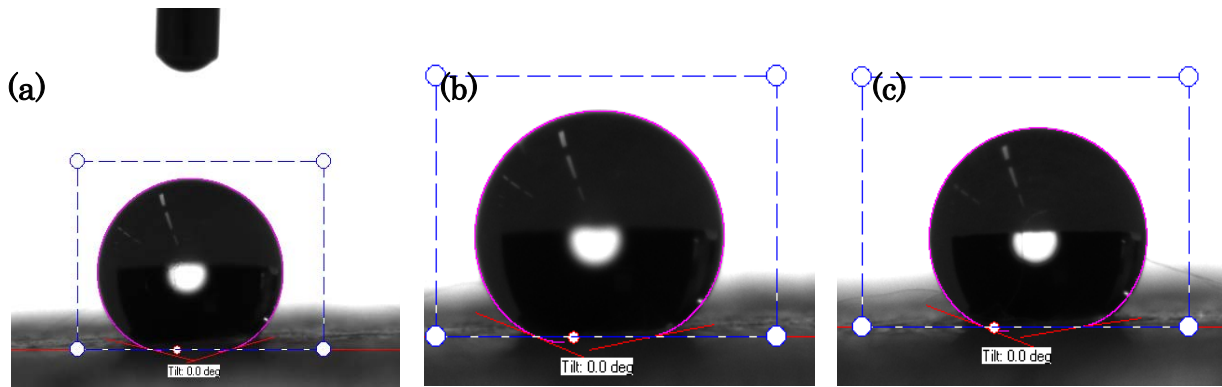


Fig. 36. Optical images of the water contact angle on the PS+ZnO sample. The WCA measurements were (a) 165.44° , (b) 163.45° and (c) 165.18° , which lead to a mean value of $\text{WCA}=165\pm 2^\circ$.

The results obtained were the expected ones, with the PVC+ZnO nanocomposite coating showing an almost superhydrophobic behaviour and the PS+ZnO having a clear superhydrophobic behaviour and exhibiting a maximum WCA of 165° . Therefore the presence of ZnO does not seem to have an important impact on the WCA of the nanocomposite electrospun film at room temperature.

5.3. Heat treatment

After the optimized electrospinning parameters were found to fulfill the proposed objectives and the zinc oxide nanoparticles were successfully incorporated into the electrospun fiber mat, the behaviour of the coatings after a thermal treatment was studied.

The main limitation found for the electrospun coatings is that they do not show a very high adherence to the substrate. This can be a constraint and reduce the implementation of this technique in industrial applications. One effective way to increase the adherence of the fiber mat onto the substrate is to perform a thermal treatment. Homaeigohar et al. found that heating of electrospun polyethersulfone fibers (PES) improves adhesion between the electrospun fibers and the underlying substrate [38]. Furthermore, several studies have shown that heat treatment is able to increase the mechanical strength of the electrospun mat. The reason for this may be that heat treatment encourages fusion at the contact points between fibers, providing a strengthening effect [39].

Heat treatment is usually carried out at temperature between the glass transition temperature (T_g) and the melting temperature (T_m) of the material. The glass transition temperature (T_g) is the temperature below which the polymer stays in glassy state (amorphous solid) and above which it presents a viscous liquid form [40].

The application of a heat treatment to the PVC and PS electrospun coatings in this work was performed with two different goals: (1) increasing the adhesion between the fibers and the underlying substrate and (2) checking the hypothesis that heating the sample above T_g would improve the ZnO nanoparticles distribution between the fibers due to the movement and vibrations of the polymer chains, thus leading to an improvement in the corrosion resistance of the coating.

Firstly the glass transition temperature of both PVC and PS was determined using differential scanning calorimetry (DSC), then thermal treatments were performed heating the samples up to various temperatures and measuring the evolution of the WCA as a function of the temperature, and finally fiber characterization using Field Emission Scanning Electron Microscopy (FE-SEM) and Atomic Force Microscopy (AFM) was performed.

5.3.1. Glass transition temperature of PVC and PS

Theoretically it is known that the glass transition temperature (T_g) of PVC is around 80 °C, and that of PS is around 100 °C. In order to corroborate this information, the T_g of electrospun PVC and PS was determined using differential scanning calorimetry (DSC). DSC is a thermoanalytical technique that measures the difference in the amount of heat required to increase the temperature of a sample and a reference, as a function of the temperature. DSC based techniques are frequently used to study and analyze the thermal properties of polymer materials [41].

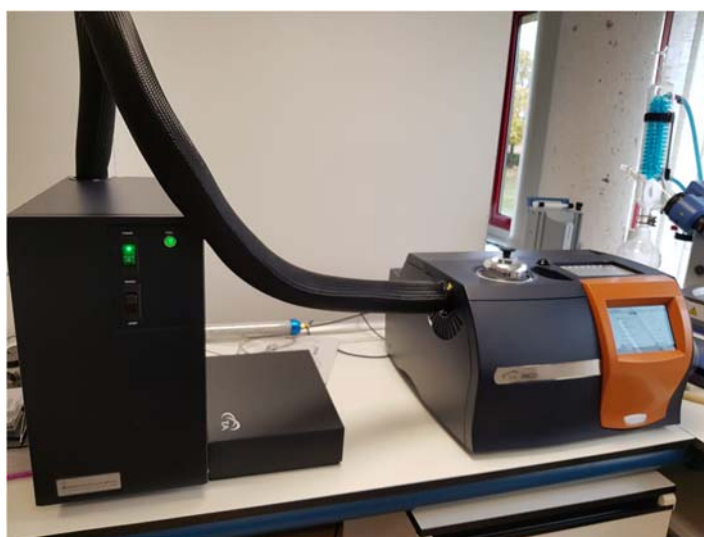


Fig. 37. Differential scanning calorimeter (right) and refrigeration unit (left) of the AIN (Asociación de la Industria Navarra), where DSC tests were performed.

Two samples of PVC fibers, with and without ZnO nanoparticles, electrospun at 14 kV and 0.6 ml/h (optimized parameters) and two samples of PS fibers, with and without ZnO nanoparticles, electrospun at 11 kV and 0.9 ml/h (optimized parameters) were studied in the AIN (Asociación de la Industria Navarra). The DSC tests were performed starting from an equilibrium temperature of -80 °C and raising 10 °C per minute up to a final temperature of 200 °C. Results obtained are shown in figures 38 and 39.

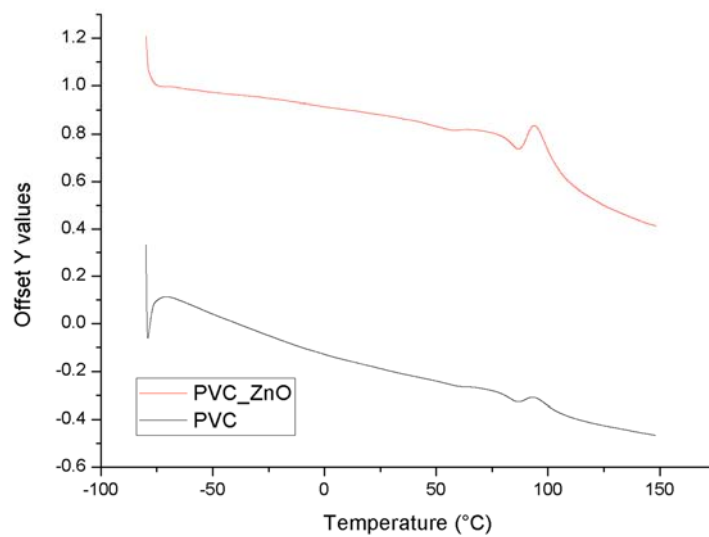


Fig. 38. DSC analysis of both PVC fibers with no corrosion inhibitor (black line) and PVC fibers containing zinc oxide nanoparticles (red line).

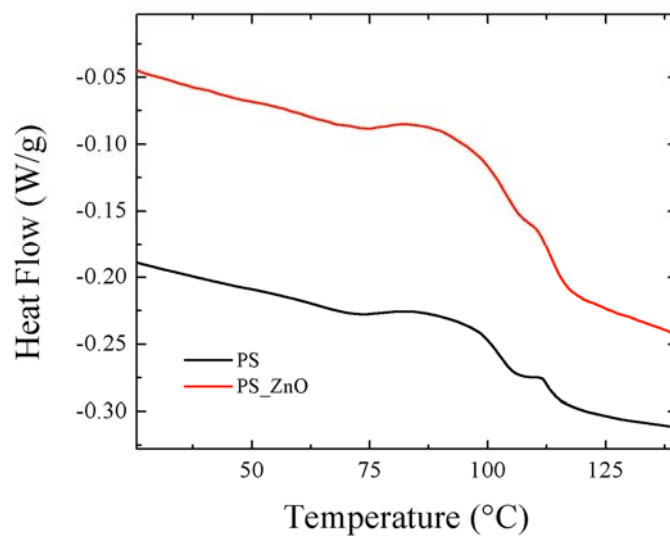


Fig. 39. DSC analysis of both PS fibers with no corrosion inhibitor (black line) and PS fibers containing zinc oxide nanoparticles (red line).

The results showed that the addition of ZnO produces an increment in the amount of heat required to increase the temperature of the electrospun fibers in both the PVC and the PS samples, but the shape of the graphs (heat flow versus temperature) remains almost equal. This means that the presence of ZnO nanoparticles in between the fiber mat does not produce a relevant change in the thermal behaviour of PVC and PS fibers; therefore the glass transition temperature is not modified.

The glass transition temperatures of PVC and PVC+ZnO were found to be 82.27 °C and 82.36 °C respectively, and the ones of PS and PS+ZnO were found to be 102.07 °C and 101.99 °C respectively, which goes in concordance with the values expected.

5.3.2. Effect of heat treatment on the water contact angle values

The effects of heat treatment on the WCA values of electrospun PVC and PS fibers at 60, 70, 80, 90 100, 110 and 120 °C were studied. One representative sample was studied for each polymer. In the case of PVC the sample analyzed was sample B from section 5.1 (*"Optimization of the electrospinning parameters"*), which was electrospun under an applied voltage of 12 kV and a flow rate of 0.8 ml/h. In the case of PS the sample analyzed was sample L from section 5.1, which was electrospun under an applied voltage of 13 kV and a flow rate of 1,5 ml/h.

Firstly, each sample was heated to the lowest heat treatment temperature (i.e. 60 °C for the PVC sample and 80 °C for the PS sample) during 1 hour in an oven, then the samples were taken out and after they were cooled down water contact angle measurements were performed. Once the WCA was determined the sample was heated again in the oven for 1 hour at the next temperature of study, that is 10 °C higher than the previous treatment, and the process was repeated until the whole range of temperatures (up to 120 °C) were covered.



Fig. 40. Oven employed for the heat treatment of the samples.

For the WCA determination three measurements were taken for each sample at three different zones and then the arithmetic mean was computed. Results are shown in table 6.

		Contact angle values at different temperatures							
		Temperature(°C)							
Sample	Polymer	Room Temp (20°C)	60	70	80	90	100	110	120
B	PVC	143	147	149	147	139	138	135	120
L	PS	159	-	-	159	162	163	137	123

Table 6. Effect of heat treatment on the water contact angle values of PVC and PS films. *Note that there are no results for PS at 60 and 70 °C, this is because the Tg of PS is 100 °C so no significant variation with respect to the WCA without heat treatment is expected at those temperatures.

The contact angle values of the PVC fiber film increased as the temperature was raised up to values close -but lower- to the glass transition temperature of PVC (i.e. 80 °C), from a minimum WCA of 143° before any heat treatment to a maximum of 149° at 70 °C. After surpassing the glass transition temperature the contact angle values of PVC started to decrease, reaching a minimum WCA of 120° after the final heat treatment at 120 °C.

Similar behaviour can be observed for the PS sample. The contact angle values slightly increased from 159° before heat treatment up to a maximum of 163° at 100 °C, which corresponds to the glass transition temperature of PS. Then after surpassing this Tg the contact angle values rapidly decreased reaching a minimum WCA of 123° after the final treatment at 120 °C. This decrease was found to be faster than the corresponding one of PVC.

These results go in accordance with the results obtained by Asmatulu et al. [30]. The change in the contact angles may be related to the rearrangement of the fiber structures in the film at the glass transition temperature. Below Tg both PVC and PS are glassy solids, and the polymer chains are rigid and cannot move. Above Tg the polymer chains start moving and vibrating, and the film becomes softer and rubbery, which may produce this decrease in the water contact angles.

The initial increase of the WCA values when approaching the Tg of the polymer may be related to the improvement of the mechanical properties with temperatures but without surpassing the glass transition temperature [39].

Figures 41 and 42 show the variation of the contact angle with temperature, for both PVC and PS.

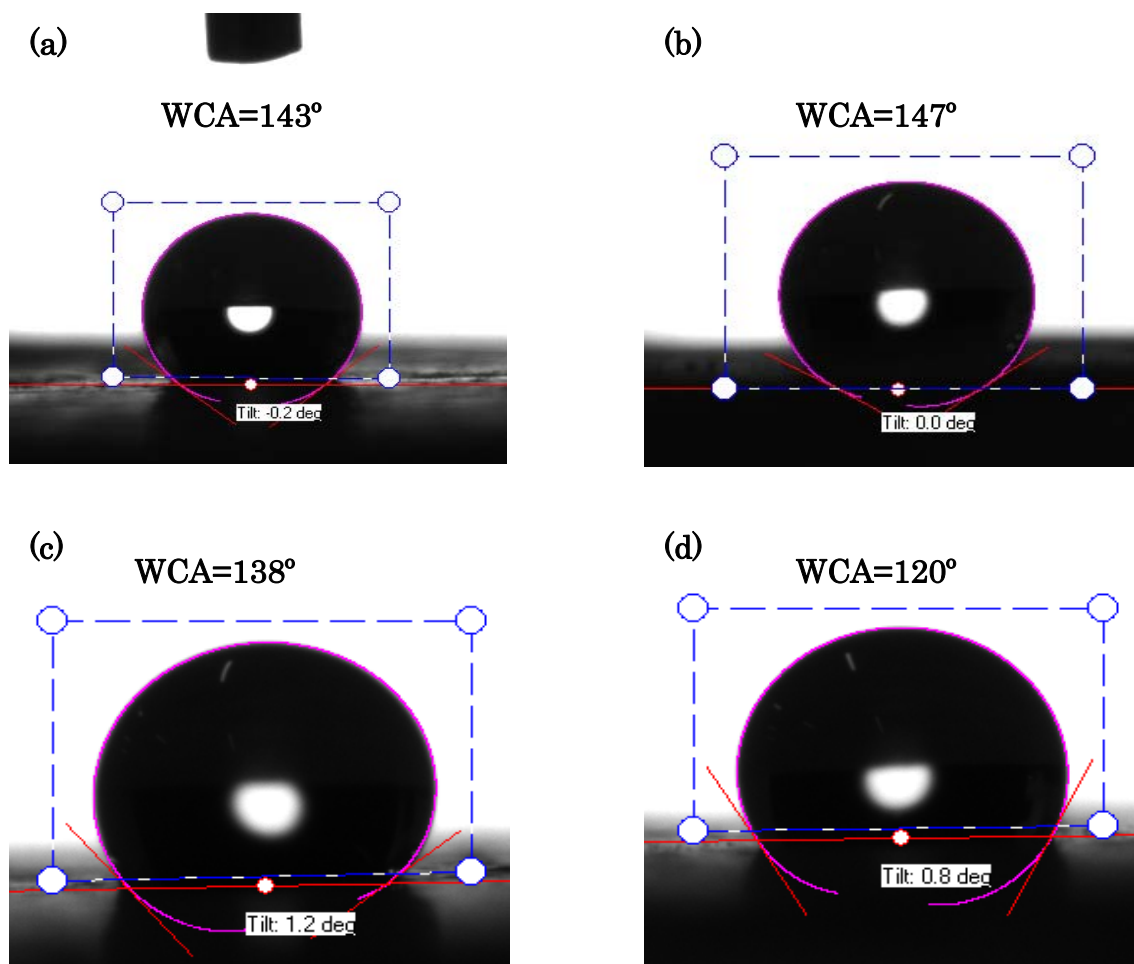


Fig. 41. Evolution of the contact angle of the PVC sample with increasing temperature. (a) Before heat treatment, (b) heated to 80 °C, (c) heated to 100 °C and (d) heated to 120 °C. The reduction of the WCA when heating over the T_g of PVC (i.e. 80 °C) can be clearly seen.

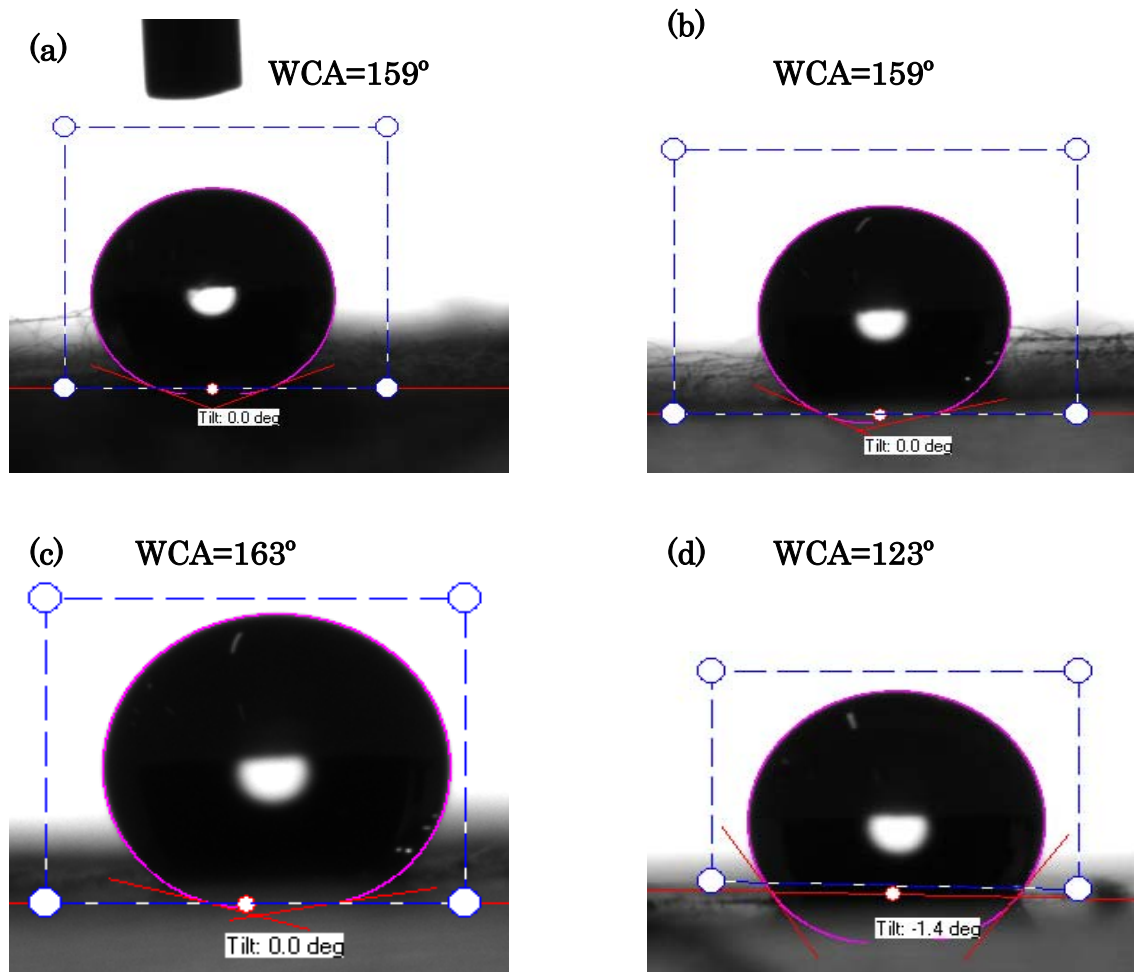


Fig. 42. Evolution of the contact angle of the PS sample with increasing temperature. (a) Before heat treatment, (b) heated to 80 °C, (c) heated to 100 °C and (d) heated to 120 °C. The reduction of the WCA when heating over the T_g of PVC (i.e. 100 °C) can be clearly seen.

As the results show, the most hydrophobic surfaces are obtained when the electrospun polymer fibers are heated up to their glass transition temperature, and exceeding the T_g point leads to a decrease in their water repellence properties. Due to this the corrosion tests were performed over samples after being heated up to T_g, and also over samples heated 20 °C over the polymer T_g in order to check the hypothesis that a better distribution of zinc oxide nanoparticles caused by the movement of the polymer chains above the glass transition temperature could compensate the contact angle decrease and improve the corrosion resistance of the coating.

5.3.3. Fiber characterization after heat treatment, AFM and SEM

Atomic force microscopy (AFM) and field emission scanning electron microscopy (FE-SEM) techniques were employed in order to characterize the morphology of the PVC and PS nanocomposite fibers containing ZnO nanoparticles after being heat-treated. The samples of PVC and PS studied were electrospun under the optimized processing parameters (i.e. 14 kV and a flow rate of 0.6 ml/h for the PVC sample, and 11 kV and a flow rate of 0.9 ml/h for the PS sample). Zinc oxide addition was done as explained in section 5.2. ("*Corrosion inhibitor (ZnO) addition*") and the samples were heated for 1 h at a temperature 20 °C higher than the glass transition point of the respective polymer (PVC sample heated to 100 °C and PS sample heated to 120 °C).

The analysis of these samples with AFM and FE-SEM techniques were performed in the AIN (Asociación de la Industria Navarra).

5.3.3.1. Atomic Force Microscopy results

- PVC:

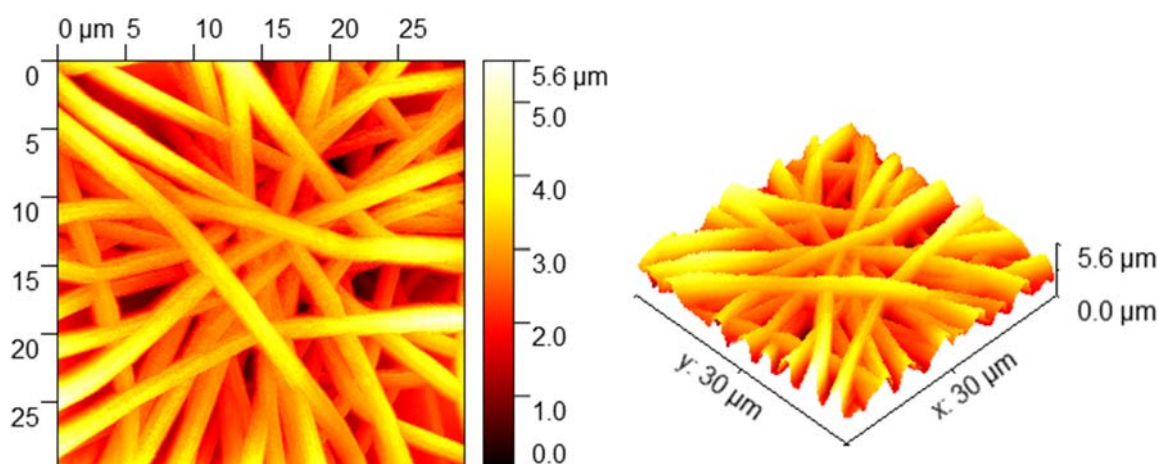


Fig. 43. AFM images of PVC sample in 2-D (left) and 3-D (right). Image dimensions: 30x30 μm. The mean fiber diameter value of 720 nm measured with the optical microscope (Table 5) seems to go in accordance with the AFM results.

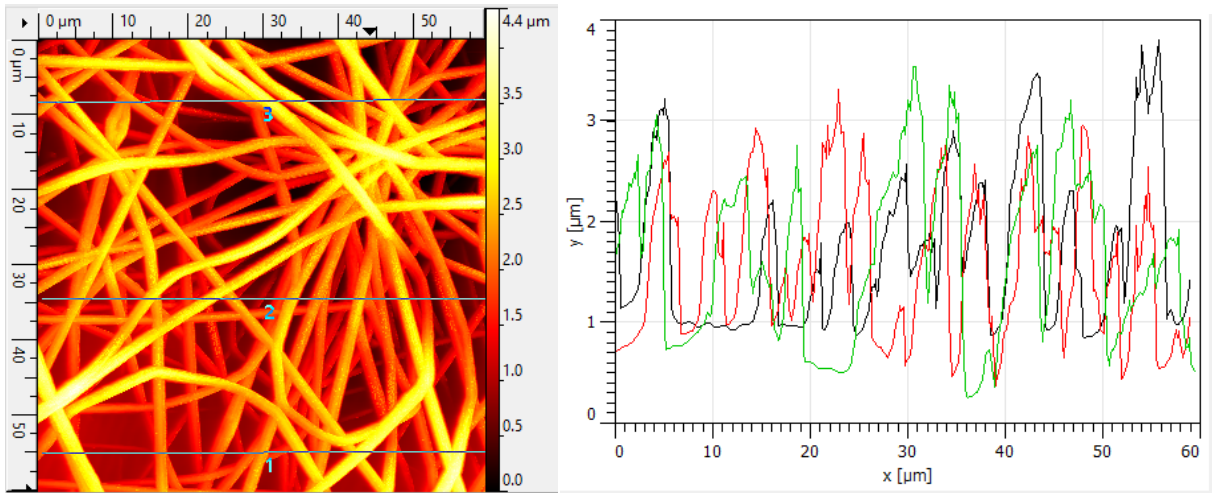


Fig. 44. On the left: 2-D AFM image of the PVC sample. Image dimensions: 60x60 μm . On the right: roughness profiles corresponding to the three evaluation lines indicated on the left. The arithmetic average roughness was found to be $R_a=427.5 \text{ nm}$.

- **PS:**

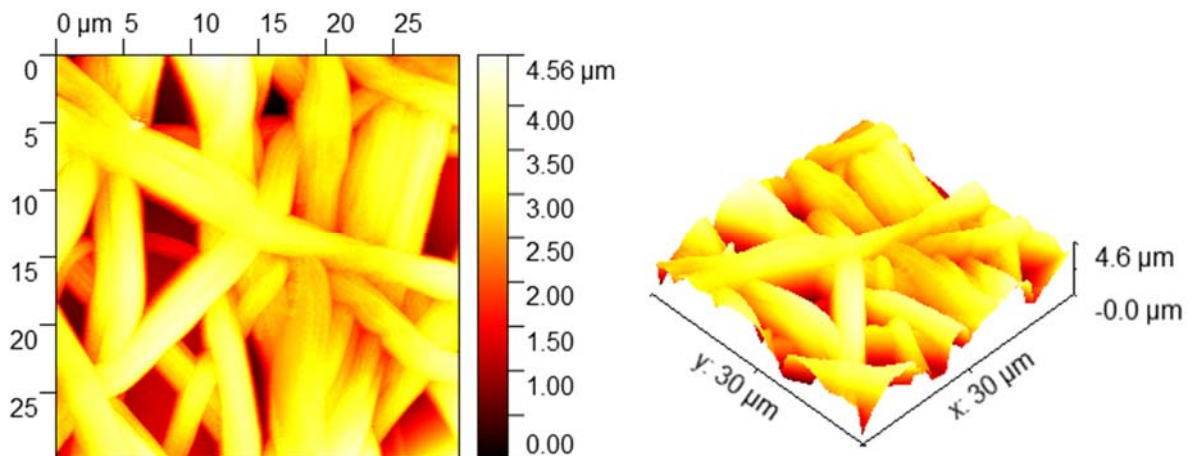


Fig. 45. AFM images of the PS sample in 2-D (left) and 3-D (right). Image dimensions: 30x30 μm . The mean fiber diameter value of 2.10 μm measured with the optical microscope (Table 5) seems to go in accordance with the AFM results.

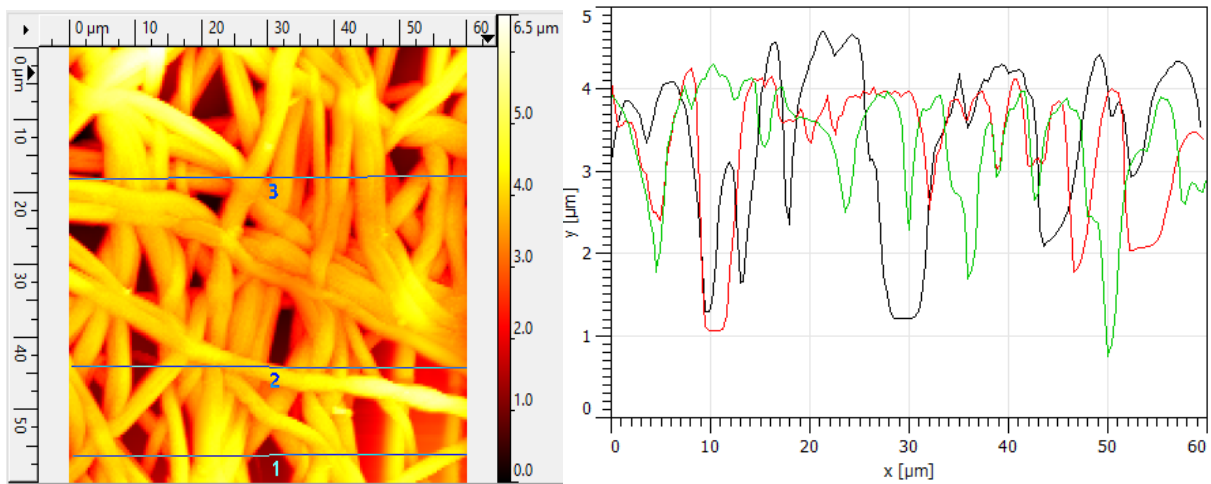


Fig. 46. On the left: 2-D AFM image of the PS sample. Image dimensions: 60x60 μm . On the right: roughness profiles corresponding to the three evaluation lines indicated on the left. The arithmetic average roughness was found to be $R_a=505.7$ nm.

The atomic force microscopy results showed that the PS electrospun coating presented a higher surface roughness than the PVC one. The arithmetic average roughness of the PS nanocomposite fibers was found to be $R_a=505.7$ nm, whereas that of the PVC fibers was measured to be $R_a=427.5$ nm. This explains the higher hydrophobicity of the PS electrospun structures compared to the PVC ones, as the Cassie-Baxter wetting model states that hydrophobicity is enhanced by the increment in surface roughness.

5.3.3.2. Scanning Electron Microscopy results

- PVC:

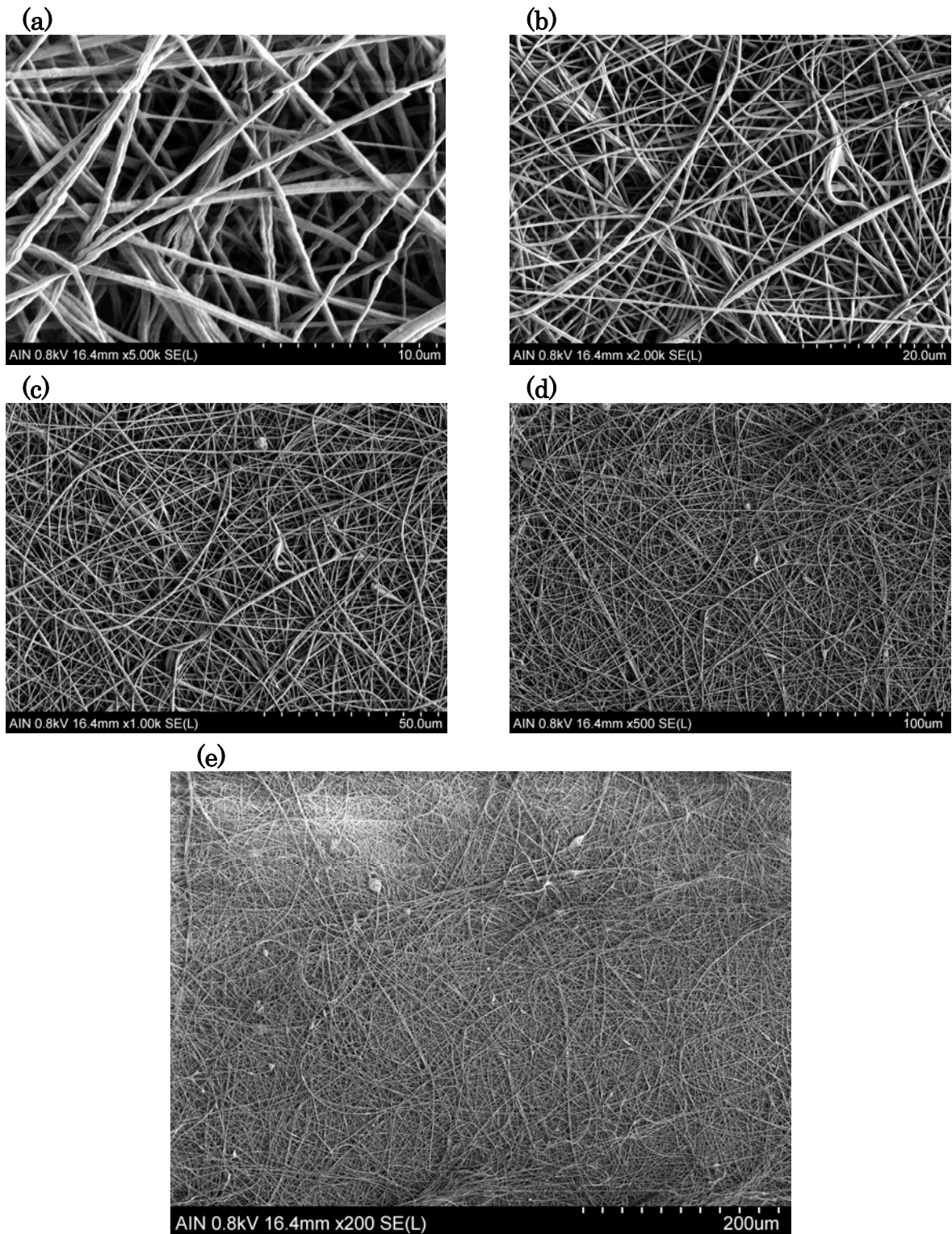


Fig. 47. SEM images of electrospun PVC nanocomposite fibers at different scales: (a) 5000x, (b) 2000x, (c) 1000x, (d) 500x and (e) 200x.

- PS:

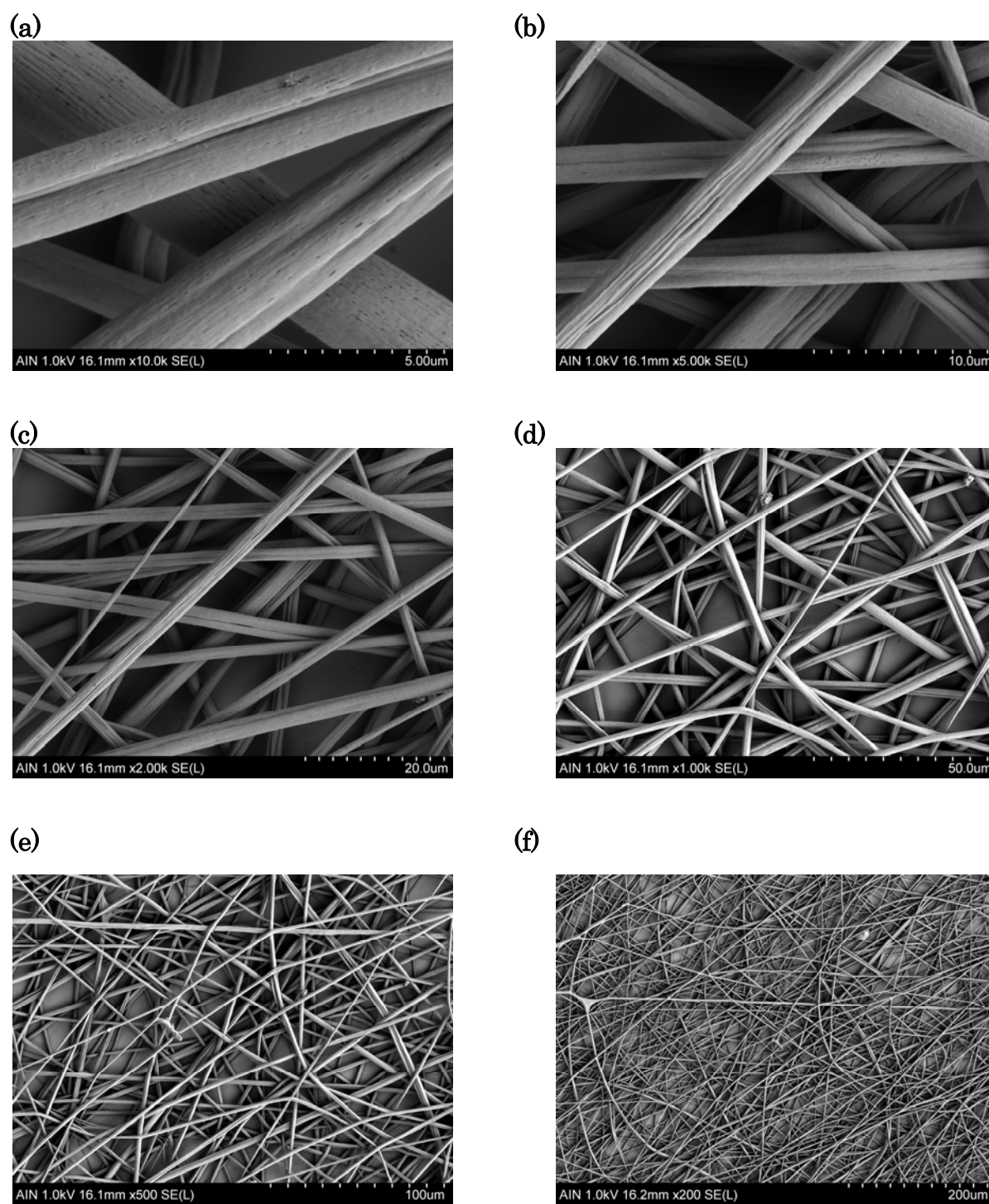


Fig. 48. SEM images of electrospun PS nanocomposite fibers at different scales: (a) 10000x, (b) 5000x, (c) 2000x, (d) 1000x, (e) 500x and (f) 200x.

5.4. Corrosion tests

The main objective of this work was the electrospinning of polymer coatings with the aim of improving the corrosion resistance of aluminum substrates. In order to check if the electrospun PVC and PS nanocomposite films successfully enhance this corrosion resistance, Tafel polarization and pitting corrosion tests were performed.

The aluminum substrate studied in this work was the alloy 6061T6. It is a precipitation-hardened aluminum alloy (AA), and further tempered, containing magnesium (Mg) and silicon (Si) as its major alloying elements. This presence of Mg and Si increase the mechanical properties of the alloy.

<u>Component</u>	<u>Wt. %</u>	<u>Component</u>	<u>Wt. %</u>	<u>Component</u>	<u>Wt. %</u>
Al	95.8 - 98.6	Mg	0.8 - 1.2	Si	0.4 - 0.8
Cr	0.04 - 0.35	Mn	Max 0.15	Ti	Max 0.15
Cu	0.15 - 0.4	Other, each	Max 0.05	Zn	Max 0.25
Fe	Max 0.7	Other, total	Max 0.15		

Table 7. Composition of aluminum alloy 6061-T6 [2].

Firstly, corrosion tests were performed over the AA 6061T6 without any coating. The results would provide a reference for the analysis of the corrosion resistance improvement after adding the electrospun nanocomposite coatings.

5.4.1. Tafel polarization test methodology

Polarization methods such as Tafel extrapolation are experimental techniques that allow to study the corrosion rate of a surface exposed to a corrosive environment in a much faster way than classical weight loss estimation techniques.

The Tafel polarization test allows the determination of the corrosion potential (E_{corr}) and the corrosion current density (i_{corr}) by the extrapolation of the cathodic and anodic Tafel slopes of the polarization curves $\{E \text{ vs } \log(i)\}$. The typical polarization behaviour of a metal in an acid solution is given in Fig. 49.

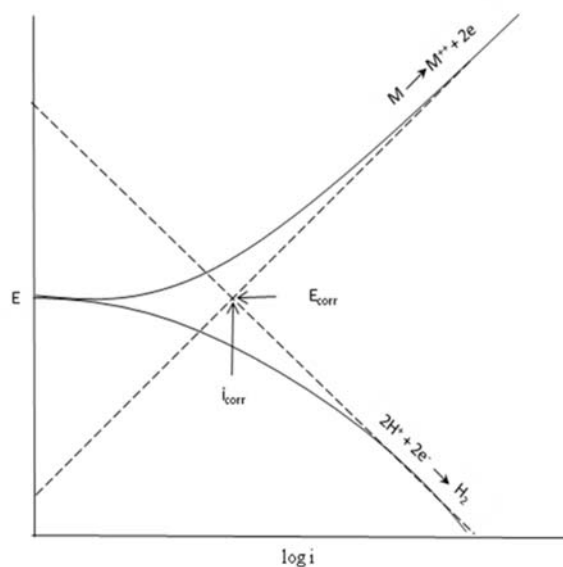


Fig. 49. Polarization behaviour of a metal (M) in acid solution [42].

At the corrosion potential, E_{corr} , the rate of the cathodic reaction is equal to the rate of the anodic reaction. Tafel constants β_a and β_c are the slopes of the anodic and cathodic curves in their linear region.

In this work all Tafel polarization tests were performed at ambient temperature in a 3.5 wt% NaCl aqueous solution, using a conventional three electrode cell consisting of a working electrode (bare or coated aluminum sample), a silver chloride Ag-AgCl reference electrode and a platinum counter electrode.

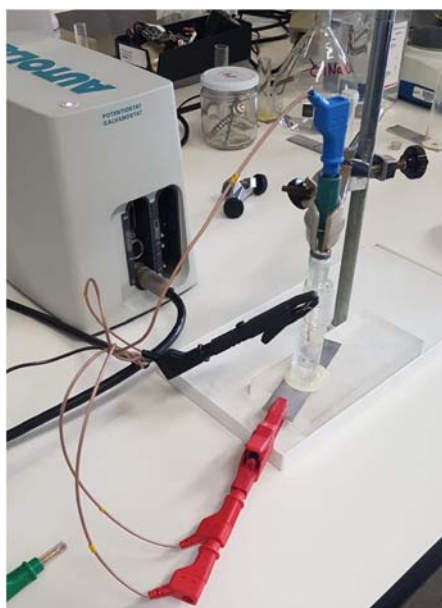


Fig. 50. Autolab potentiostat used for the Tafel and pitting corrosion tests.

Before conducting the Tafel polarization experiments all the samples were immersed in the 3.5 wt% NaCl electrolyte for 20 minutes. Then, the Tafel tests start with the stabilization of the open circuit potential (OCP) until $dE/dt < 10^{-6}$ V/s. After that, Tafel polarization measurements were obtained by scanning the electrode potential from -150 mV to $+150$ mV at a scan rate of 1.5 mV/s and steps of 0.5 mV. Finally the Tafel analysis provides the resulting values of the polarization slopes β_a and β_c , the corrosion current density (i_{corr}) and the corrosion potential (E_{corr}).

5.4.2. Pitting corrosion test methodology

Once the Tafel polarization tests were performed pitting corrosion tests were conducted in order to determine the behaviour of bare aluminum and coated aluminum against pitting (localized) corrosion. All pitting corrosion tests were performed at ambient temperature and with the same 3.5 wt% NaCl solution. Also the same potentiostat and the three-electrode cell configuration were used.

After the to-be-studied sample was immersed in the 3.5 wt% NaCl electrolyte for 20 minutes, the open circuit potential was determined. Once the OCP was stabilized ($dE/dt < 10^{-6}$ V/s) the pitting test was conducted starting the measurements at an initial electric potential equal to OCP. Measurements were taken with a scan rate of 0.15 mV/s and with increasing voltage steps of 0.15 mV. Once the current intensity surpassed the cutoff value of 2.5 mA the scan direction was reversed.

Pitting corrosion tests allow for the determination of the point where pitting appear (E_p), i.e. the electric potential above which the corrosion current starts increasing very rapidly.

5.4.3. Corrosion tests results for bare aluminum

Firstly, corrosion tests were performed over a bare sample of the aluminum alloy 6061T6 without any coating. The results would provide a reference for the analysis of the corrosion resistance improvement after adding the electrospun nanocomposite coatings of PVC and PS. Figures 51 and 52 show the Tafel polarization curves and pitting corrosion results of the bare aluminum sample.

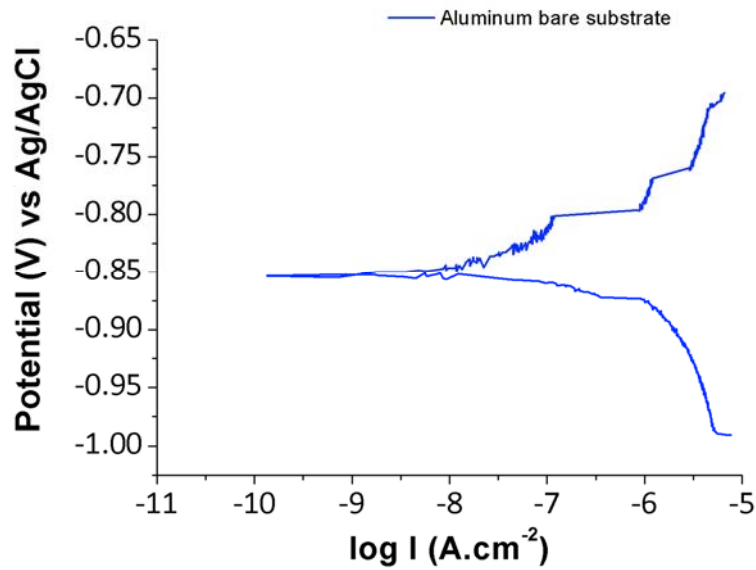


Fig. 51. Tafel plot for the aluminum bare substrate in 3.5 wt% NaCl aqueous solution.

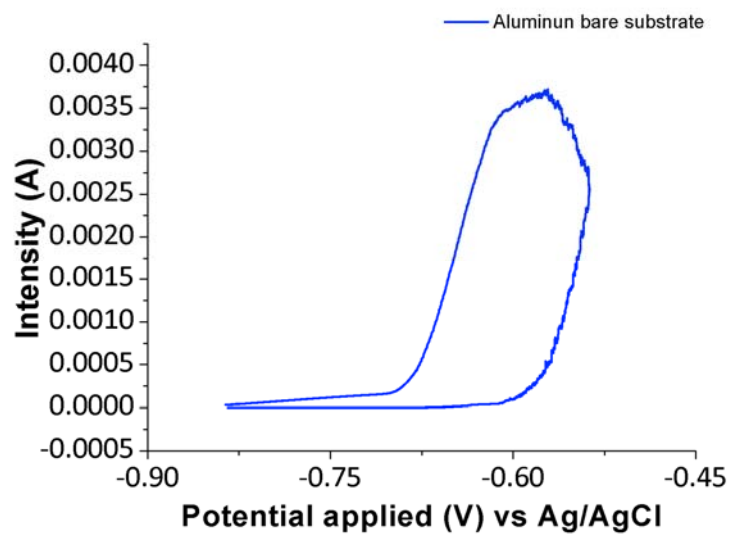


Fig. 52. Pitting corrosion curve for the aluminum bare substrate in 3.5 wt% NaCl aqueous solution.

The Tafel analysis results showed that the corrosion current density for the aluminum alloy was $1.107 \mu\text{A cm}^{-2}$ at a corrosion potential of -0.856 V , and the cathodic and anodic Tafel constants were found to be 150 and 56 mV/decade respectively.

The pitting corrosion curve provides information about the bare aluminum behaviour against localized (pitting) corrosion. Scully et al. defined the pitting potential E_p as the potential above which the rising current permanently exceeded $10 \mu\text{A}$ [43]. Therefore following that definition the pitting potential of the bare aluminum sample was found to be -0.656 V .

After corrosion tests were successfully conducted over the reference bare aluminum sample, the corrosion behaviour of aluminum coated with the electrospun polymer films was studied in order to see if there was an improvement in the corrosion resistance of the metallic substrate with the use of these nanocomposite coatings.

5.4.4. Corrosion tests results for the PVC nanocomposite coatings

For testing the corrosion resistance of the electrospun PVC films in the presence and absence of nanoparticle inclusions four samples were produced, two of them composed only of PVC fibers and the other two containing zinc oxide nanoparticles. The four samples were electrospun using the optimized processing parameters corresponding to PVC (i.e. voltage of 14 kV and flow rate of 0.6 ml/h), and this time the fibers were deposited onto the aluminum 6061T6 slide. In order to improve the adherence between the polymer fibers and the metallic substrate, a plasma treatment was applied to the aluminum slides for 10 minutes before the electrospinning process.

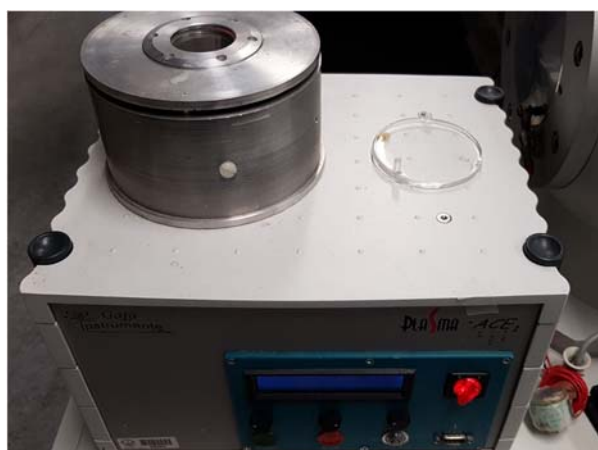


Fig. 53. Plasma treatment machine.

After the four samples were successfully electrospun they were subjected to heat treatment. Two samples, one containing only PVC fibers and the other one containing also ZnO nanoparticles, were heated at 80 °C for 1 hour, and the remaining two samples (with and without ZnO) were heated to 100 °C for 1 hour. These temperatures were chosen because 80 °C is the glass transition temperature (T_g) of PVC and at this temperature the nanocomposite coating exhibits the highest water contact angle (see table 6), and the temperature of 100°C (T_g+20) is chosen with the aim of studying whether a better distribution of the ZnO nanoparticles could compensate the decrease in the water contact angle and improve the corrosion performance.



Fig. 54. Aluminum slide coated with electrospun PVC fibers before being heat-treated.

Tafel polarization tests were performed over the four samples following the methodology explained in section 5.4.1. (*"Tafel polarization test methodology"*). The Tafel plots are displayed in figure 55 and the results are shown in table 8.

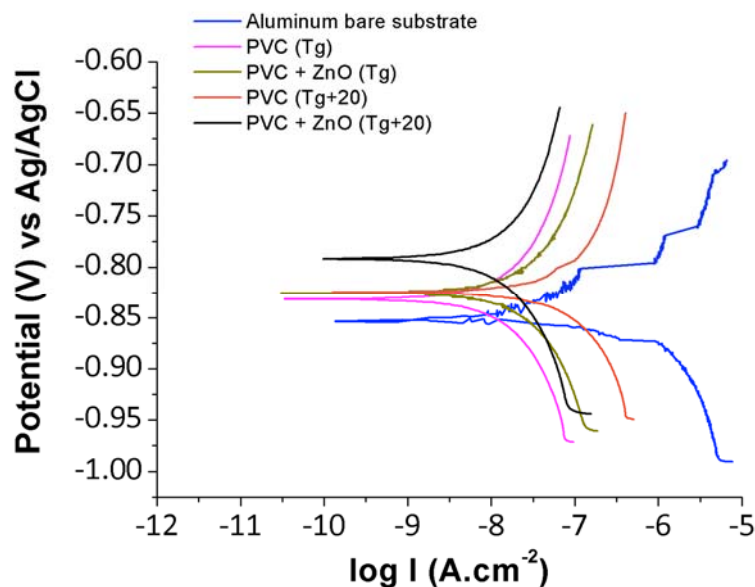


Fig. 55. Tafel plots for the Al bare substrate and for the four Al samples coated with electrospun PVC fibers in 3.5 wt% NaCl aqueous solution.

sample	β_a (mV/dec)	β_c (mV/dec)	i_{corr} ($\mu\text{A}/\text{cm}^2$)	E_{corr} (V)	efficiency (%)
Al substrate	56	150	1.107	-0.856	-
PVC (Tg)	155	143	0.011	-0.833	99.01
PVC (Tg+20)	197	172	0.029	-0.827	97.38
PVC+ZnO (Tg)	140	96	0.054	-0.826	95.12
PVC+ZnO (Tg+20)	175	159	0.009	-0.793	99.19

Table 8. Tafel analysis for uncoated Al substrate, pure PVC and PVC+ZnO composite coatings after being heat-treated, tested in 3.5 wt% NaCl aqueous solution.

The results show that all electrospun coatings reduced the corrosion current of the aluminum in two orders of magnitude. This corrosion resistance was lowered significantly from $1.107 \mu\text{A cm}^{-2}$ in the case of bare Al to a minimum of $0.009 \mu\text{A cm}^{-2}$ in case of Al/PVC+ZnO after being heat treated to 100°C (Tg+20).

The corrosion potential was displaced towards less negative values, attaining a maximum of -0.793 V in the case Al/PVC+ZnO (Tg+20) again.

The protection efficiency for the coatings was calculated with the same methodology as [9,44,45]:

$$efficiency (\%) = \frac{i_1 - i_2}{i_1} \times 100\%$$

where i_1 and i_2 correspond to the corrosion current densities of the bare Al and the coated one respectively.

The protection efficiency in the case of pure PVC after being heat-treated to 80 °C (T_g) was found to be 99.01%. When the pure PVC coating was heated to 100 °C the efficiency was reduced to 97.38%, which can be explained by the decrease in the water contact angle when surpassing the glass transition temperature of the polymer. The composite coating of PVC+ZnO presented lower efficiency than the other samples when heated to T_g , but it was found that when this composite coating was heated 20 degrees higher than T_g the protection efficiency reached a maximum of 99.19%, which may be related to a better distribution of zinc oxide nanoparticles.

As the composite coating of PVC+ZnO heat-treated to 100 °C presented the best anti-corrosion properties in the Tafel polarization tests, its behaviour against pitting corrosion was also tested.

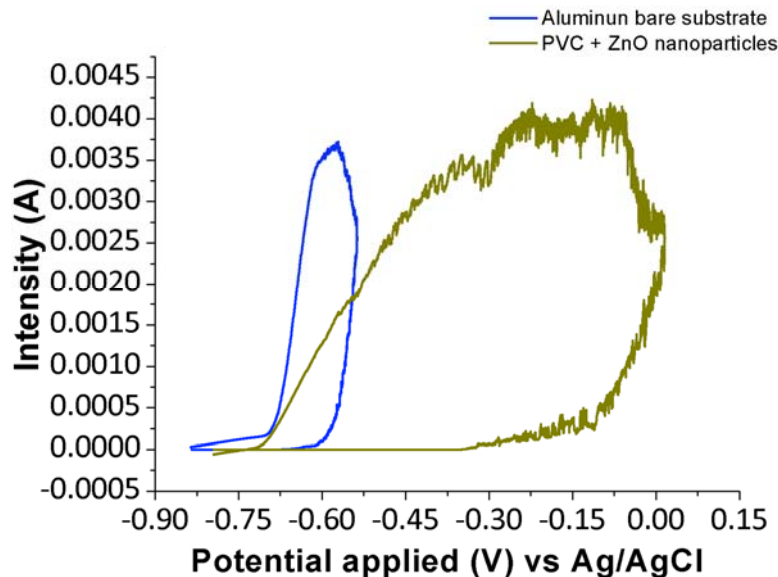


Fig. 56. Pitting test plots for the bare Al substrate and the composite PVC+ZnO coating tested in 3.5 wt% NaCl aqueous solution.

Figure 56 shows that the resistance against pitting corrosion was clearly enhanced by the nanocomposite electrospun coating. Its pitting potential (i.e. the potential above which the rising current permanently exceeded 10 μ A [43]) was found to be -0.341 V, which is closer to positive values than the pitting potential of bare Al which was -0.656 V. This means that higher electric potential is needed in order for pitting corrosion to appear in the composite coating. Furthermore, once pitting starts it grows with a slower rate. The current cutoff of 2.5 mA was found to be reached under a potential of 0.015 V in the case of the PVC+ZnO coating, while it was reached way before, at -0.538 V, in case of bare Al.

5.4.5. Corrosion tests results for the PS nanocomposite coatings

For testing the corrosion resistance of the electrospun PS films in the presence and absence of nanoparticle inclusions the same methodology used for the PVC analysis was followed, but for this case only three samples were produced, one of them composed only of PS fibers and the other two containing zinc oxide nanoparticles. The reason for this is that the coating composed only by PS fibers will only be studied after being heat-treated to the glass transition temperature of PS (i.e. 100 °C), because surpassing this Tg leads to a big decrease in the water contact angle: from 163° at 100 °C down to 123° at 120°C (the WCA in the case of PVC did not suffer such a fast decrease when surpassing the Tg of the polymer, see table 6). Such a reduction in the hydrophobic character is not desired.

The three samples were electrospun using the optimized processing parameters corresponding to PS (i.e. voltage of 11 kV and flow rate of 0.9 ml/h) and they were deposited onto the aluminum 6061T6 slides. A plasma treatment was again performed to the Al substrate prior to the electrospinning process in order to improve the adherence of the PS electrospun fibers.

Before conducting the corrosion tests, heat treatments were carried out: the Al/PS sample was heated to 100 °C (Tg) for 1 hour, and the Al/PS+ZnO composite samples were heated to 100 °C and 120 °C (Tg+20) each.

Tafel polarization tests were performed over the three samples following the methodology explained in section 5.4.1. ("*Tafel polarization test methodology*"). The Tafel plots are displayed in figure 57 and the results are shown in table 9.

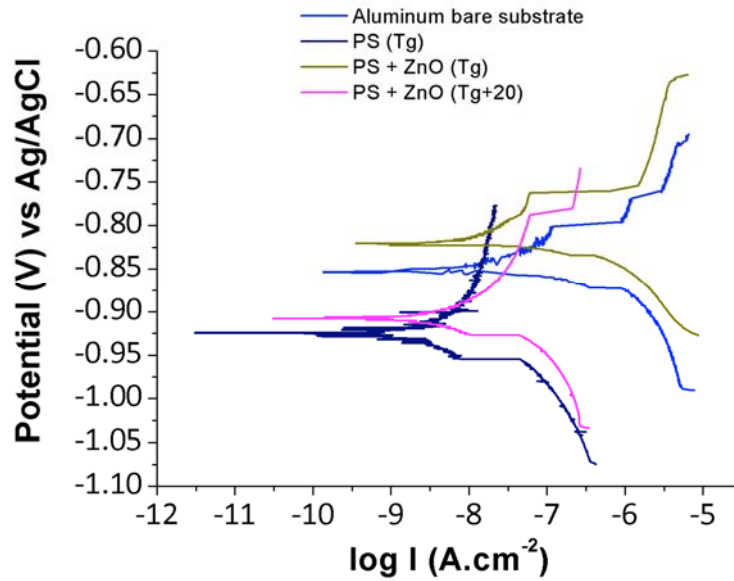


Fig. 57. Tafel plots for the Al bare substrate and for the Al samples coated with electrospun PS fibers in 3.5 wt% NaCl aqueous solution.

sample	β_a (mV/dec)	β_c (mV/dec)	i_{corr} ($\mu\text{A}/\text{cm}^2$)	E_{corr} (V)	efficiency (%)
Al substrate	56	150	1.107	-0.856	-
PS (Tg)	217	99	0.013	-0.927	98.83
PS+ZnO (Tg)	71	67	0.067	-0.822	93.95
PS+ZnO (Tg+20)	101	97	0.010	-0.909	99.10

Table 9. Tafel analysis for uncoated Al substrate, pure PS and PS+ZnO composite coatings after being heat-treated, tested in 3.5 wt% NaCl aqueous solution.

The results show that all electrospun coatings reduced the corrosion current of the aluminum in two orders of magnitude. This corrosion resistance was lowered significantly from $1.107 \mu\text{A cm}^{-2}$ in the case of bare Al to a minimum of $0.010 \mu\text{A cm}^{-2}$ in case of Al/PS+ZnO after being heat treated to 120°C (Tg+20).

For the corrosion potential, a clear trend cannot be deduced because while the nanocomposite coating of PS+ZnO heat-treated to Tg displaced E_{corr} towards more positive values, the other two samples produced a displacement of E_{corr} towards more negative values.

In the case of the protection efficiency for the coatings the same behaviour as in the PVC analysis can be observed: the composite coating PS+ZnO presented lower efficiency than the pure PS coating when heated to the glass transition temperature of the polymer (see table 8), but it was found that when this composite coating was heated 20 degrees higher than Tg the protection efficiency reached a maximum value of 99.10%, which may be related to a better distribution of zinc oxide nanoparticles.

As the composite coating of PS+ZnO heat-treated to 120 °C presented the best anti-corrosion properties in the Tafel polarization tests, its behaviour against pitting corrosion was also tested.

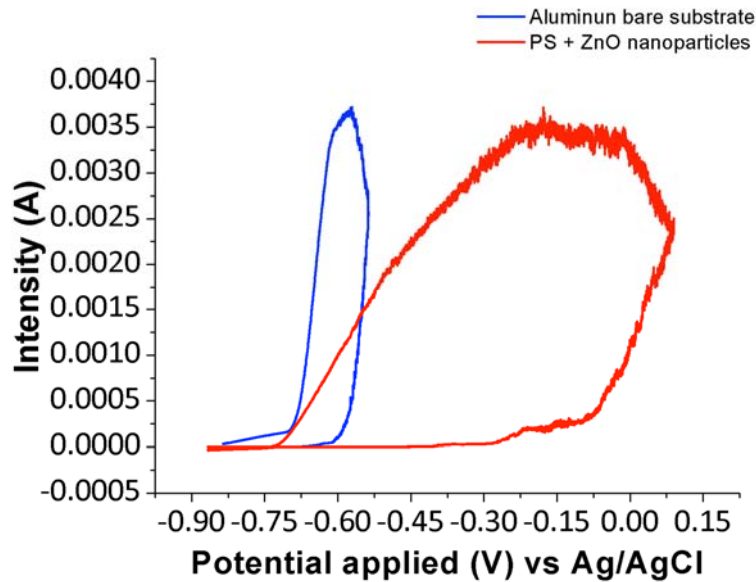


Fig. 58. Pitting test plots for the bare Al substrate and the composite PS+ZnO coating tested in 3.5 wt% NaCl aqueous solution.

Figure 58 shows that the resistance against pitting corrosion was again clearly enhanced by the nanocomposite electrospun coating. The pitting potential of this coated sample was found to be -0.398 V, which is closer to positive values than the pitting potential of bare Al (i.e. -0.656 V). This means that higher electric potential is needed in order for pitting corrosion to appear in the composite coating. Furthermore, once pitting starts it grows with a much slower rate. The current cutoff of 2.5 mA was found to be reached at 0.090 V in the case of PS+ZnO coating, while it was reached at -0.538 V in case of bare Al.

5.4.6. Overall pitting corrosion tests results

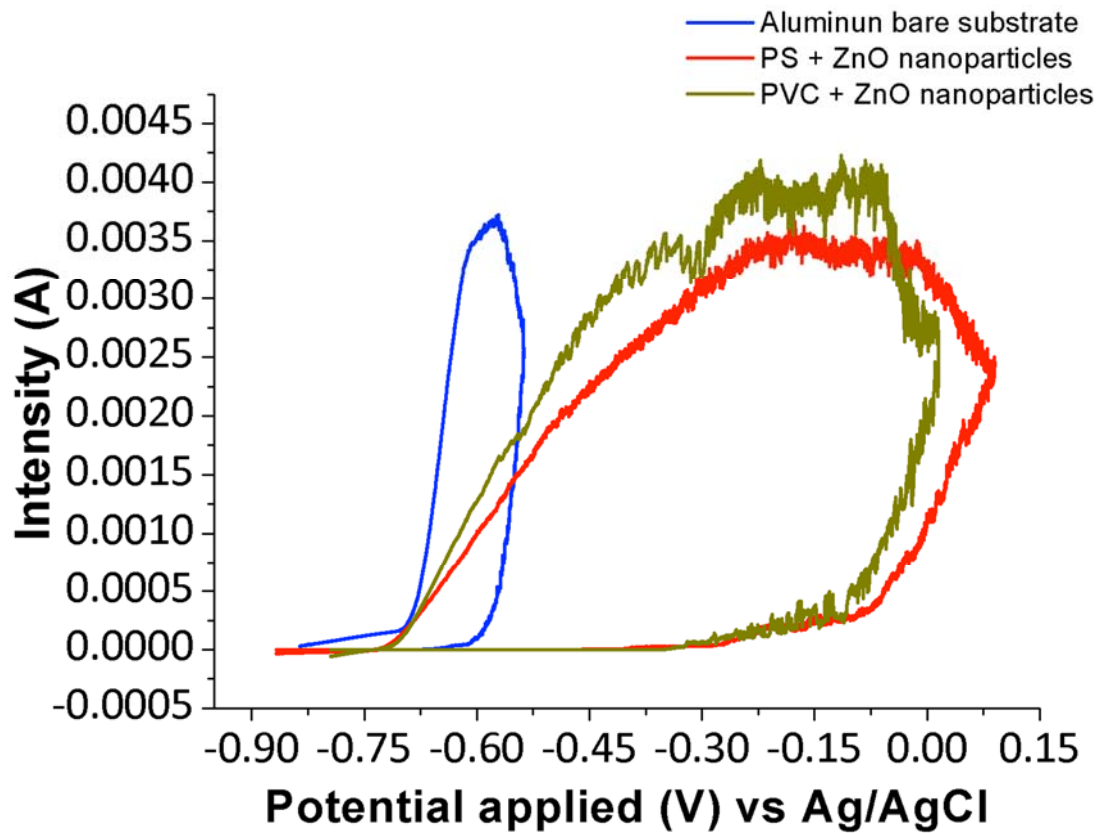


Fig. 59. Pitting test plots for the bare Al substrate and the composite PVC+ZnO and PS+ZnO coatings tested in 3.5 wt% NaCl aqueous solution.

Figure 59 shows how both polymer coatings successfully improve the pitting resistance of the aluminum alloy. The pitting current increase rate can be estimated as the slope of the polarization curve between the pitting potential (E_p) and the electric potential at the 2.5 mA current cutoff point (E_{cutoff}). This can be approximated using the following equation:

$$i_{corr} = \frac{2.5 - 10 \times 10^{-3}}{E_{cutoff} - E_p} \text{ (mA/V)}$$

Sample	E_p (V)	E_{cutoff} (V)	i_{corr} (mA/V)
Al substrate	-0.656	-0.538	21.10
PVC+ZnO (Tg+20)	-0.341	0.015	6.99
PS+ZnO (Tg+20)	-0.398	0.090	5.10

Table 10. Pitting test results for the bare Al substrate and the composite PVC+ZnO and PS+ZnO coatings tested in 3.5 wt% NaCl aqueous solution.

The pitting test results showed that pitting starts before (at more negative applied electric potentials) in the PS nanocomposite coating, but the rate of increase of the pitting current is higher in the PVC nanocomposite coating. Either way, both electrospun coatings proved to improve significantly the corrosion resistance of the aluminum alloy against pitting corrosion.

**CHAPTER 6:
CONCLUSIONS AND
FUTURE RESEARCH
LINES**

CONCLUSIONS

In summary, it has been demonstrated that electrospun nanocomposite coatings of both PVC and PS improve the corrosion resistance of the aluminum alloy 6061T6 due to the high hydrophobic character of the resulting surfaces, even excellent superhydrophobicity with WCA higher than 160° was obtained for PS coatings, which may be explained by the high roughness of these surfaces.

Nanocomposite films of PVC and PS containing ZnO nanoparticles were successfully prepared using one-step electrospinning technique. The effect of heat-treating these coatings was also analyzed. The heat treatments improved the adhesion between the electrospun fibers and the underlying substrate, and the corrosion tests revealed that heating the nanocomposite polymer+ZnO structures 20 degrees higher than the glass transition temperature of the polymer allows obtaining excellent anti-corrosion behaviour. This may be explained by a better distribution of the ZnO nanoparticles due to the movement of the polymer chains above T_g , which compensates for the decrease in the hydrophobic behaviour of the fibers at such high temperatures.

Tafel polarization tests showed that the corrosion current density could be reduced in two orders of magnitude with the use of these electrospun coatings and pitting corrosion tests also demonstrated that the nanocomposite surfaces enhance the resistance of aluminum against localized corrosion.

FUTURE RESEARCH LINES

Electrospinning is still a novel fiber production technique and the field of future development is very wide. For a better understanding of the process a Design of Experiments (DOE) methodology could be performed in order to study the variation of the output variables of the process, such as fiber diameter or pore size, as a function of the input or independent variables, such as applied voltage, flow rate and solution concentration. There is not much literature, if any, about a DOE carried out for the electrospinning technique so this is a potential future research field.

The main limitation for the use of electrospun polymer fibers as anti-corrosion coatings in metallic substrates seems to be the adherence between the electrospun film and the metallic surface, which is not very high. Therefore the study of different heat treatments and other techniques that may help improving this adherence has special interest and might be a potential research field.

Finally, the corrosion inhibitor employed in this work has been ZnO. There are researches about blending a polymer with inorganic and organic nanomaterials, but most of them are focused on adding just one type of inhibitor. Another possible future research line is the study of the utilization of more than one corrosion inhibitor at the same time.

**CHAPTER 7:
PUBLICATIONS IN
INTERNATIONAL
CONFERENCES**

5th Global Nanotechnology Congress and Expo

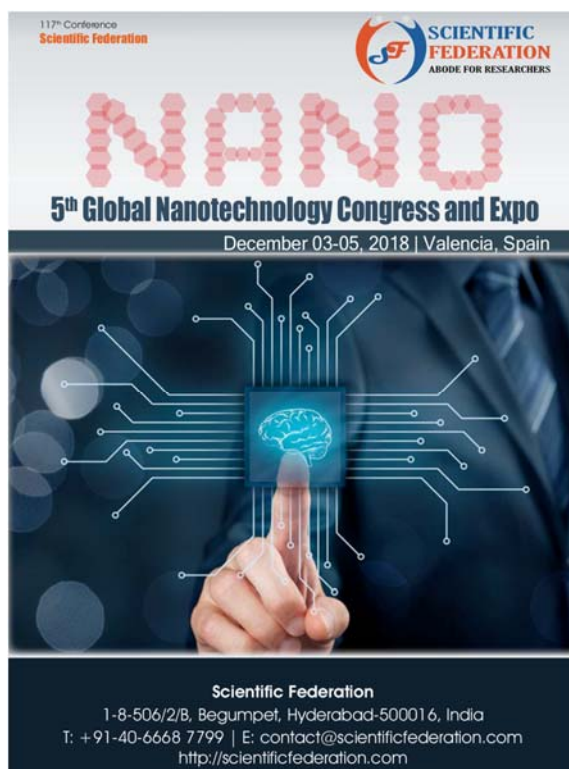



Fig. 60. Cover for the 5th Global Nanotechnology Congress and Expo, held in Valencia, Spain.

**SCIENTIFIC
FEDERATION**
ABODE FOR RESEARCHERS

5th Global Nanotechnology Congress and Expo

December 03-05, 2018 | Valencia, Spain

Implementation of Functionalized Ps Electrospun Nanofibers onto Aluminium Substrates for the Design of Superhydrophobic and Anticorrosive Nanocoatings

Pedro Jose Rivero Fuente^{1,2}, A Iribarren¹, C Berlanga^{1,2}, J Goicoechea³ and R Rodriguez^{1,2}

¹Materials Science Laboratory, Engineering Department, Public University of Navarra (UPNA), Spain
²INAMAT – Institute for Advanced Materials, Public University of Navarra (UPNA), Spain
³Sensors Laboratory, Electrical and Electronic Department, Public University of Navarra (UPNA), Spain

In this work, the combination of metal oxide precursors with electrospun PS fibers have successfully been deposited onto Aluminium substrates (6061T6) for the design of functionalized coatings with an enhancement of the resultant corrosion resistance and mechanical properties. Several characterization tests have been performed, including Field Emission Scanning Electron Microscopy (FE-SEM), Atomic Force Microscopy (AFM), Term gravimetric analysis (TGA), Optical Microscopy (OM), Water contact angle (WCA) measurements and corrosion polarization tests (Tafel curves). Finally, an exhaustive study of the mechanical properties of the thin films by using scratching test has been carried out in order to corroborate the benefit of incorporating these metal oxide precursors into the electrospun fibers.

Fig. 61. Literature review of the work published in the 5th Global Nanotechnology Congress and Expo.

Implementation of functionalized PS electrospun nanofibers onto aluminium substrates for the design of superhydrophobic nanocoatings

ABSTRACT

In this work, the combination of metal oxide precursors with electrospun PS fibres have successfully been deposited onto aluminium substrates (6061T6) for the design of functionalized coatings with an enhancement of the corrosion resistance and mechanical properties. Several characterization tests have been performed, including Field Emission Scanning Electron Microscopy (FE-SEM), Atomic Force Microscopy (AFM), Thermogravimetric analysis (TGA), Optical Microscopy (OM), Water contact angle (WCA) measurements and corrosion polarization tests (Tafel curves). Finally, an exhaustive study of the mechanical properties of the thin films by using scratching test has been carried out in order to corroborate the benefit of incorporating these metal oxide precursors into the electrospun fibers.

RESULTS AND DISCUSSION

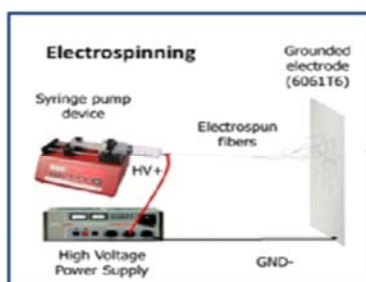


Figure 1: setup experimental for electrospinning process.

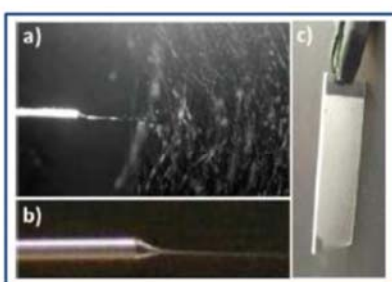


Figure 2: electrospun fibers onto the cathode and aspect of the coating.

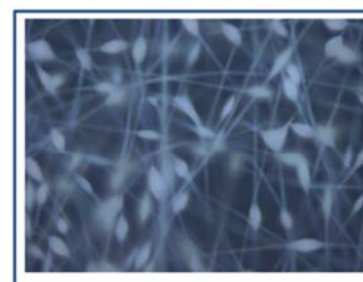


Figure 3: optical microscopy image of the PS electrospun fibers

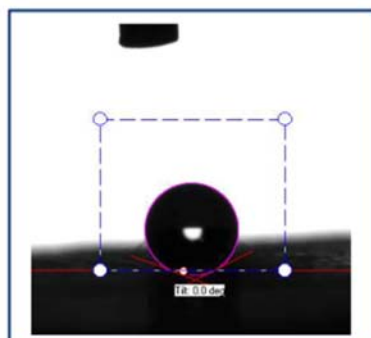


Figure 4: water contact angle (WCA) measurement of the electrospun fibers

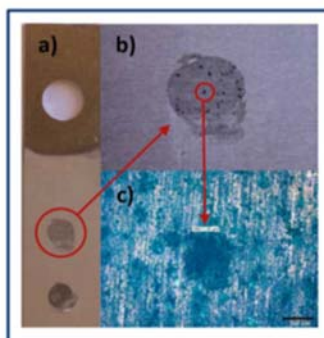


Figure 5: aspect of the pitting marks after potentiodynamic tests.

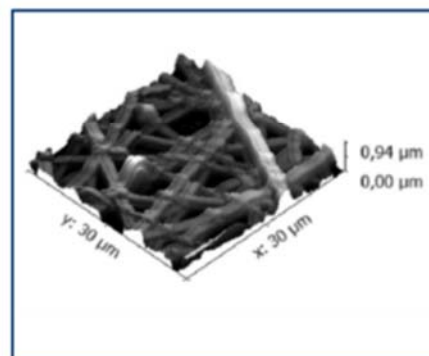


Figure 6: AFM image of the PS electrospun coatings

ACKNOWLEDGEMENTS

This work was supported by the Spanish Economy and Competitiveness Ministry - FEDER Proyecto Retos TRA2013-48603-C4-1-R and by the Public University of Navarra collaboration research grants. The authors would like to express their gratitude to Nadetech Inc. for the tune-up of the robot used for the deposition of the nanocoatings.

REFERENCES

- (1) Maeztu, J. D.; Rivero, P. J.; Berlanga, C.; Bastidas, D. M.; Palacio, J. F.; Rodríguez, R. Effect of Graphene Oxide and Fluorinated Polymeric Chains Incorporated in a Multilayered Sol-Gel Nanocoating for the Design of Corrosion Resistant and Hydrophobic Surfaces. *Appl. Surf. Sci.* 2017, 419, 138-149.
- (2) Covelo, A.; Genescá, J.; Barba, A.; Menchaca, C.; Uruchurtu, J.; Hernández, M. Corrosion Behavior of Hybrid Sol-Gel Films Reinforced with Electrospun Nanofibers. *Solid State Phenomena* 2015, 227, 119-122.
- (3) Liu, X.; Gu, C.; Wen, Z.; Hou, B. Improvement of Active Corrosion Protection of Carbon Steel by Water-Based Epoxy Coating with Smart CeO₂ nanocontainers. *Prog Org Coatings* 2018, 115, 195-204.

Fig. 62. Poster published in the 5th Global Nanotechnology Congress and Expo.

1st Coatings and Interfaces Web Conference



Sciforum

Dear Alvaro Iribarren,

We are pleased to inform you that your abstract has been approved by our editorial team.

Please make sure to upload your submission files before the full submission deadline. You can access your submission through the link below:

Submission ID: sciforum-022950

Title: Implementation of superhydrophobic PS electrospun nano/microfibers for corrosion protection of aluminum substrates

Authors: Alvaro Iribarren *, Pedro J. Rivero, Carlos Berlanga, José F. Palacio, Silvia Larumbe, Javier Goicoechea, Rafael Rodríguez

Conference: 1st Coatings and Interfaces Web Conference

Section: Posters

Editor decision: Approve

Editor comments:

<https://sciforum.net/dashboard/author/submissions/ef43a15e2094434c75b3ad61d1a557cb>

Kind regards,

Your CIWC2019 Organizing Team

ciwc2019@sciforum.net

Fig. 63. Confirmation of approved abstract for the 1st Coatings and Interfaces Web Conference.

Conference	1st Coatings and Interfaces Web Conference
Session	Posters
Submission details	
Article ID	sciforum-022950
Status	abstract accepted
Title	Implementation of superhydrophobic PS electrospun nano/microfibers for corrosion protection of aluminum substrates
Authors	Alvaro Iribarren *, Pedro J. Rivero, Carlos Berlanga, José F. Palacio, Silvia Larumbe, Javier Goicoechea, Rafael Rodríguez
Abstract	In this work, the electrospinning technique is used for the synthesis of micro/nanofibers using a polymeric precursor with hydrophobic (even superhydrophobic) behaviour such as polystyrene (PS) or polyvinyl chloride (PVC). These electrospun fibers are deposited onto aluminum substrates (6061T6). The effect of varying the different electrospinning deposition parameters (mostly applied voltage and flow-rate) will be exhaustively analyzed in order to optimize the resultant electrospun coatings. Several fiber characterization tests have been performed, including Field Emission Scanning Electron Microscopy (FE-SEM), Atomic Force Microscopy (AFM), Termogravimetric analysis (TGA), Optical Microscopy (OM) and Water Contact Angle (WCA) measurements. Furthermore, the anti-corrosion properties of these electrospun coatings can be enhanced by the addition of metal oxide nanoparticles (ZnO) which act as corrosion inhibitors. Finally, electrochemical corrosion tests (Tafel and pitting tests) have been performed, showing an improvement in the resultant corrosion resistance of the aluminum alloys coated by the combination of both polymeric film with metal oxide inorganic nanoparticles.
Keywords	Electrospinning, superhydrophobic, metal oxide nanoparticles, corrosion

Fig. 64. Abstract submitted to the 1st Coatings and Interfaces Web Conference.

Acknowledgements

The author would like to express his grateful acknowledgement for the support and kind treatment received from the Asociación de la Industria Navarra (AIN). Thanks are also due to José F. Palacio for assistance with the AFM analysis and to Silvia Larumbe for assistance with the TGA and DSC analyses.

Finally, thanks due to my tutors Dr. Pedro J. Rivero and Dr. Carlos Berlanga, and to Dr. Javier Goicoechea for their support and willingness.

REFERENCES

- [1] M. Abdel-Gaber, B.A. Abd-El-Nabey, I.M. Sidahmed, A.M. El-Zayady, M. Saadawy, Kinetics and thermodynamics of aluminium dissolution in 1.0 M sulphuric acid containing chloride ions, *Mater. Chem. Phys.* 98 (2006) 291.
- [2] ASM Handbook, Volume 2: Properties and Selection: Nonferrous Alloys and Special-Purpose Materials ASM Handbook Committee, p 102 DOI: 10.1361/asmhba0001060
- [3] W.A. Badawy, F.M. Al-Kharafi, A.S. El-Azab, Electrochemical behaviour and corrosion inhibition of Al, Al-6061 and Al-Cu in neutral aqueous solutions, *Corros. Sci.* 41 (1999) 709.
- [4] Stansbury, E. and Buchanan, R. (2000). *Introduction and Overview of Electrochemical Corrosion*. [ebook] Available at: <https://www.asminternational.org/documents/10192/3466254/ACFA9DE.pdf/acf8d808-336a-4636-aadf-80b7e2092398> [Accessed 28 Dec. 2018].
- [5] NACE International. *Corrosion Costs and Preventive Strategies in the United States*. [ebook] Available at: <https://www.nace.org/uploadedfiles/publications/ccsupp.pdf> [Accessed 28 Dec. 2018].
- [6] Alfed.org.uk. (2018). *Aluminium and Corrosion*. [online] Available at: <http://www.alfed.org.uk/files/Fact%20sheets/2-aluminium-and-corrosion.pdf> [Accessed 28 Dec. 2018].
- [7] NACE International (2018). *Pitting Corrosion*. [online] Nace.org. Available at: <https://www.nace.org/pitting-corrosion/> [Accessed 31 Dec. 2018].
- [8] M. Ates, A review on conducting polymer coatings for corrosion protection, *J. Adhes. Sci. Technol.* 30 (2016) 1510–1536.
- [9] Bahgat Radwan, A., Adel M.A. Mohamed, Aboubakr M. Abdullah and Mariam A. Al-Maadeed (2015). *Corrosion protection of electrospun PVDF-ZnO superhydrophobic coating*.
- [10] W.Y. Gan, S.W. Lam, K. Chiang, R. Amal, H. Zhao, M.P. Brungs, Novel TiO₂ thin film with non-UV activated super wetting and antifogging behaviours, *J. Mater. Chem.* 17 (2007) 952.
- [11] M.Nicolas, F.Guittard, S.Geribaldi, Stable superhydrophobic and lipophobic conjugated polymers films, *Langmuir* 22 (2006) 3081.
- [12] R.Taurino, E.Fabbri, M.Messori, F.Pilati, D.Pospiech, A.Synytsk, Facile preparation of superhydrophobic coatings by sol-gel processes, *J. Colloid Interface Sci.* 325 (2008) 149.
- [13] S.Amigoni, E.P.T.Givenchy, M.Dufay, F.Guittard, Covalent layer-by-layer assembled superhydrophobic organic-inorganic hybrid films, *Langmuir* 25 (2009) 11073.
- [14] K. Acatay, E. Simsek, C. Ow-Yang, Y.Z. Menceloglu, Tunable, superhydrophobically stable polymeric surfaces by electrospinning, *Angew. Chem. Int. Ed.* 43 (2004) 5210.

- [15] A.B.D. Cassie, S. Baxter, Wettability of porous surfaces, *Trans. Faraday Soc.* 40 (1944) 546.
- [16] Travis J. Sill and Horst A. von Recum (2008). *Electrospinning: Applications in drug delivery and tissue engineering*.
- [17] Yarin AL, Koombhongse S, Reneker DH. Bending instability in electrospinning of nanofibers. *J Appl Phys* 2001 Mar 1;89(5):3018-26.
- [18] Deitzel JM, Kleinmeyer J, Harris D, Tan NCB. The effect of processing variables on the morphology of electrospun nanofibers and textiles. *Polymer* 2001 Jan;42(1):261-72. □
- [19] Megelski S, Stephens JS, Chase DB, Rabolt JF. Micro- and nanostructured surface morphology on electrospun polymer fibers. *Macromolecules* 2002 Oct 22;35(22):8456-66. □
- [20] Doshi J, Reneker DH. Electrospinning process and applications of electrospun fibers. *J Electrostatics* 1995 Aug;35(2-3):151-60. □
- [21] Baumgarten P. Electrostatic spinning of acrylic microfibers. *J Colloid Interface Sci* 1971;36(1):71-9.
- [22] P. J. Rivero, A. Urrutia, J. Goicoechea, Y. Rodríguez, J. M. Corres, F. J. Arregui and I. R. Matías (2012). An Antibacterial Submicron Fiber Mat with In Situ Synthesized Silver Nanoparticles.
- [23] Lowry, T. and Richardson, K. (1987). *Mechanism and theory in organic chemistry*. New York: Harper & Row, p.177.
- [24] McMurry, J., Zendejas Escandón, A., Macías Pérez, M., Gómez Macías, A. and Trujillo Chávez, G. (2012). *Química orgánica*. Cengage Learning Editores, p.383.
- [25] Liu, W., Huang, C. and Jin, X. (2015). Electrospinning of Grooved Polystyrene Fibers: Effect of Solvent Systems. *Nanoscale Research Letters*, 10(1).
- [26] A.M.A. Mohamed, R. Jafari, M. Farzaneh, An optimization of superhydrophobic polyvinylidene fluoride/zinc oxide materials using Taguchi method, *Appl. Surf. Sci.* 288 (2014) 229.
- [27] Hallaji, H., Keshtkar, A. and Moosavian, M. (2015). A novel electrospun PVA/ZnO nanofiber adsorbent for U(VI), Cu(II) and Ni(II) removal from aqueous solution. *Journal of the Taiwan Institute of Chemical Engineers*, 46, pp.109-118.
- [28] Vitchuli, N., Shi, Q., Nowak, J., Kay, K., Caldwell, J., Breidt, F., Bourham, M., McCord, M. and Zhang, X. (2011). Multifunctional ZnO/Nylon 6 nanofiber mats by an electrospinning-electrospraying hybrid process for use in protective applications. *Science and Technology of Advanced Materials*, 12(5), p.055004.
- [29] Ma, M; Mao, Y; Gupta, M; Gleason, K. K.; Rutledge, G. C. *Macromolecules* 2005, 38, 9742.
- [30] Asmatulu, R., Ceylan, M. and Nuraje, N. (2011). Study of Superhydrophobic Electrospun Nanocomposite Fibers for Energy Systems. *Langmuir*, 27(2), pp.504-507.

- [31] Dreval', V., Tager, A., Sycheva, É. and Vzvadskaya, Z. (1973). Effect of the molecular weight of polystyrene on the viscosity of concentrated solutions. *Polymer Mechanics*, 6(5), pp.795-800.
- [32] Paul, Hiemenz C., and Lodge P. Timothy. *Polymer Chemistry*. Second ed. Boca Raton: CRC P, 2007. 336, 338–339.
- [33] Reneker DH, Chun I (1996) Nanometre diameter fibres of polymer, produced by electrospinning. *Nanotechnology* 7(3):216–223. doi:10.1088/0957-4484/7/3/009
- [34] Bakar, S., Fong, K., Eleyas, A. and Nazeri, M. (2018). Effect of Voltage and Flow Rate Electrospinning Parameters on Polyacrylonitrile Electrospun Fibers. *IOP Conference Series: Materials Science and Engineering*, 318, p.012076.
- [35] Yuan X, Zhang Y, Dong C, Sheng J (2004) Morphology of ultrafine polysulfone fibers prepared by electrospinning. *Polym Int* 53(11):1704–1710. doi:10.1002/pi.1538
- [36] Huan, S., Liu, G., Han, G., Cheng, W., Fu, Z., Wu, Q. and Wang, Q. (2015). Effect of Experimental Parameters on Morphological, Mechanical and Hydrophobic Properties of Electrospun Polystyrene Fibers. *Materials*, 8(5), pp.2718-2734.
- [37] Coats, A. and Redfern, J. (1963). Thermogravimetric analysis. A review. *The Analyst*, 88(1053), p.906.
- [38] Homaeigohar, S., Koll, J., Lilleodden, E. and Elbahri, M. (2012). The solvent induced interfiber adhesion and its influence on the mechanical and filtration properties of polyethersulfone electrospun nanofibrous microfiltration membranes. *Separation and Purification Technology*, 98, pp.456-463.
- [39] Zhang, L., Liu, L., Pan, F., Wang, D. and Pan, Z. (2012). Effects of Heat Treatment on the Morphology and Performance of PSU Electrospun Nanofibrous Membrane. *Journal of Engineered Fibers and Fabrics*, 7(2_suppl), p.155892501200702.
- [40] Jadhav, N., Gaikwad, V., Nair, K. and Kadam, H. (2009). Glass transition temperature: Basics and application in pharmaceutical sector. *Asian Journal of Pharmaceutics*, 3(2), p.82.
- [41] Drzeżdżon, J., Jacewicz, D., Sielicka, A. and Chmurzyński, L. (2019). Characterization of polymers based on differential scanning calorimetry based techniques. *TrAC Trends in Analytical Chemistry*, 110, pp.51-56.
- [42] Kyanos, S. (2019). *Lecture 10: Polarization Techniques – Corrosion Rate Determination NPTEL Web Course 1 Course Title: Advances in Corrosion Engineering Course Co-ordinator: Polarization Techniques – Corrosion Rate Determination*. [online] Academia.edu. Available at: http://www.academia.edu/8385289/Lecture_10_Polarization_Techniques_Corrosion_Rate_Determination_NPTEL_Web_Course_1_Course_Title_Advances_in_Corrosion_Engineering_Course_Co-ordinator_Polarization_Techniques_Corrosion_Rate_Determination [Accessed 16 Jan. 2019].
- [43] Scully, J., Budiansky, N., Tiwary, Y., Mikhailov, A. and Hudson, J. (2008). An alternate explanation for the abrupt current increase at the pitting potential. *Corrosion Science*, 50(2), pp.316-324.

- [44] Zhao, Y., Zhang, Z. and Yu, L. (2016). Corrosion protection of carbon steel by electrospun film containing polyaniline microfibers. *Reactive and Functional Polymers*, 102, pp.20-26.
- [45] Zhao, Y., Xing, C., Zhang, Z. and Yu, L. (2017). Superhydrophobic polyaniline/polystyrene micro/nanostructures as anticorrosion coatings. *Reactive and Functional Polymers*, 119, pp.95-104.